Mihalevich Bryce, A (Orcid ID: 0000-0001-5492-221X)
Neilson Bethany, T. (Orcid ID: 0000-0001-8829-5082)
Yackulic Charles, B. (Orcid ID: 0000-0001-9661-0724)

Water temperature controls for regulated canyon-bound rivers

Bryce A. Mihalevich [1], Bethany T. Neilson [1], Caleb A. Buahin [1], Charles B. Yackulic [2], John C. Schmidt [3]

[1] Utah Water Research Laboratory, Department of Civil and Environmental Engineering, Utah State University, 8200 Old Main Hill, Logan, Utah, 84322-8200, United States
[2] U.S. Geological Survey, Southwest Biological Science Center, Grand Canyon Monitoring and Research Center, 2255 N. Gemini Dr., Flagstaff, AZ 86001, United States
[3] Department of Watershed Sciences, Utah State University, 8200 Old Main Hill, Logan, Utah 84322-8200, United States

Correspondence to: Bryce A. Mihalevich, Civil and Environmental Engineering, Utah State University, Logan, UT 84321, USA (bryce.mihalevich@aggiemail.usu.edu)

Key points:

- Topographic shading greatly reduces shortwave radiation in canyon-bound rivers
- Controls on shortwave radiation elevates the importance of flow and other typically smaller heat fluxes
- Factors that influence the downstream rate of temperature change in canyon-bound systems are highly variable over space and time

Abstract

Many canyon-bound rivers have been dammed and downstream flow and water temperatures modified. Climate change is expected to cause lower storage in reservoirs and warmer release temperatures, which may further alter downstream flow and thermal regimes. To anticipate potential future changes, we first need to understand the dominant heat transfer mechanisms in canyon-bound river systems. Towards this end, we adapt a dynamic process-based river routing and temperature model to account for complex shading and radiation characteristics found in canyon-bound rivers. We apply the model to a 362 km segment of the Colorado River in Grand Canyon National Park, USA to simulate temperature over an 18-year period. Extensive temperature and flow datasets from within the canyon were used to assess model performance. At the most downstream gaging location, root mean square errors of hourly flow routing and temperature predictions were 11.5 m^3/s and 0.93 °C, respectively. We found that heat fluxes controlling temperatures were highly variable over space and time, primarily due to shortwave radiation dynamics and hydropeaking flow conditions. Additionally, the large differences between air and water temperature during summer periods resulted in high sensible and latent heat fluxes. Sensitivity analyses indicate that reservoir release temperatures are most influential above the RM88 gage (141 kilometers below Glen Canyon Dam), while a combination of discharge, shortwave radiation, and air temperature become more important farther downstream. This study illustrates the importance of understanding the spatial and temporal variability of topographic shading when predicting water temperatures in canyon-bound rivers.

This article has been accepted for publication and undergone full peer review but has not been through the copyediting, typesetting, pagination and proofreading process which may lead to differences between this version and the Version of Record. Please cite this article as doi: 10.1029/2020WR027566

Index Terms

1. 0744 [Rivers]
2. 1847 [Modeling]
3. 1814 [Energy Budgets]
4. 1871 [Surface water quality]
5. 1857 [Reservoirs (surface)]

Keywords

1. Heat flux
2. Water temperature
3. Hydropeaking
4. Modeling
5. Topographic shading
6. Canyons

1. Introduction

Temperature plays a key role in aquatic ecosystems by driving rates of chemical reactions and resulting physiological processes, synchronizing phenological processes, and modifying trophic interactions in food webs (Olden & Naiman, 2010). As such, understanding how temperature may respond to changes in climate and hydrology is important for predicting ecosystem responses. Process-based river temperature models allow for the quantification of individual heat fluxes and the identification of dominant mechanisms, allowing for robust, temperature predictions. Because these models are built on heat transfer fundamentals that are driven by instream flow conditions and local meteorological information, they also provide insights regarding the sensitivity of river temperatures to anticipated future conditions. Many types of river systems have been studied and models adapted to represent their unique aspects including radiation from adjacent rock cliffs (e.g., Cardenas et al., 2014), surface and subsurface transient storage heat contributions (e.g., King & Neilson, 2019; Neilson et al., 2010), and longwave radiation from terrain and riparian vegetation visible from the water surface (e.g., Leach & Moore, 2010). However, the mechanisms controlling water temperatures when shortwave radiation is reduced due to significant topographic shading are not as well understood.

In deep canyons, topography obstructs direct shortwave radiation from reaching the water surface during a large portion of each day. The timing of this shading is highly dependent on the orientation of the river section, the latitude, and the day of the year (Yard et al., 2005). Many river temperature models incorporate the effects of shading from vegetation or land surfaces by scaling shortwave radiation by shading factors. These shading factors are often estimated from physical observations or land surface elevation models and can vary from constant shade factors applied over entire reaches to hourly values for specific coordinates (Chen et al., 1998a; Loinaz et al., 2013; Rutherford et al., 1997; Wawrzyniak et al., 2017). However, less attention has been given to the spatiotemporal dynamics of shading in deep canyons, which can be highly variable over relatively small scales, and therefore become important when investigating thermal regimes of canyon-bound rivers over different seasons.

When considering radiation influences in natural systems, it is common to focus on direct solar radiation and less emphasis has been given to the lower energy, diffuse component. The diffuse fraction consists of shortwave radiation that has been absorbed and

scattered within the atmosphere before reaching the land or water surface (Dubayah & Rich, 1995). In the context of process-based river temperature modeling, the diffuse shortwave radiation has at times been estimated using a fixed ratio (e.g., 20% or 30%) of the total incoming shortwave radiation (Rutherford et al., 1997; Westhoff et al., 2007). Others have used more complex empirical formulations to estimate diffuse radiation from extraterrestrial radiation and atmospheric transmissivity (Cox & Bolte, 2007; Sridhar et al., 2004) or based on a clearness index (Chen et al., 1998a; Leach & Moore, 2010; Zhang et al., 2018). Despite this heat flux often being negligible, in canyon-bound rivers the diffuse component can be the only source of shortwave radiation for extended periods of time (Stanitski-Martin, 1996; Yard et al., 2005).

Also inherent in systems with complex topography is the reduction in the atmospheric longwave radiation that reaches the water surface. Longwave radiation is an important heat source to most river systems (Caissie, 2006; Webb et al., 2008), but is reduced if a large portion of the sky is obstructed by topography or riparian vegetation (Moore et al., 2014). This decrease in atmospheric longwave radiation will increase the relative importance of longwave radiation contributed by the surrounding terrain (Cardenas et al., 2014; Matzinger et al., 2003; Plüss & Ohmura, 1997) or overhanging canopy (Leach & Moore, 2010; Roth et al., 2010). The importance of radiation emitted from surrounding topography has been shown for cirque walls of mountainous areas that re-emit longwave radiation resulting in greater incoming longwave radiation and a subsequent increase in the rates of alpine snowmelt (Brazel & Marcus, 1987; Olyphant, 1986). In the Glen Canyon portion of the Colorado River, Stanitski-Martin (1996) found that surrounding walls absorbed shortwave and longwave radiation during the day and the re-emitted longwave radiation from rock walls resulted in increased energy received at the water surface. These findings, combined with the recent emphasis on the importance of incorporating longwave radiative fluxes from landscape features (Moore et al., 2014) suggests that river temperature models applied in settings with complex topography need to be adapted to account for radiation influences from a variety of sources.

In addition to the complex radiative dynamics, canyon-bound rivers may also be affected by water development (e.g., large upstream reservoirs) which changes the natural downstream hydrologic and thermal characteristics (Collier et al., 1996; Graff, 1999; Lowney, 2000), and by extension, the downstream aquatic ecosystems (Nilsson & Renöfält, 2008; Olden & Naiman, 2010; Ward & Stanford, 1983). Reservoir release volumes can have large daily fluctuations because of power demands, resulting in higher volume releases during the daytime when demand increases and lower volume releases at night when demand decreases. This affects the thermal inertia of the river (Anderson & Wright, 2007; Carron, 2000; Webb & Walling, 1993), a property that describes the amount of energy required to alter temperatures given the volume of water in the system (Gu et al., 1998). Depending on the pattern, magnitude, and timing of releases, upstream discharge and water temperature can affect river segments that may be 100's of kilometers downstream (Carron & Rajaram, 2001; Ferencz et al., 2019). Lastly, the river surface area to volume ratio also influences downstream temperatures (Polehn & Kinsel, 1997; Risley et al., 2010). In canyon-bound rivers where the rating relation between river stage and discharge is typically steep (Wenzel & Fishel, 1942), large changes in flow may result in relatively small changes in surface area because the channel width is confined by bedrock. Therefore, the surface area available to exchange heat remains relatively constant while discharges can change significantly.

Despite the importance of canyon-bound rivers for water supply, and inherent ecosystem challenges below dammed rivers, there is limited information about which heat fluxes control temperatures in these settings or how this may change with future climate and management practices. We hypothesize that heat fluxes responsible for controlling river

temperature in regulated, canyon-bound rivers during high and low flows are highly dependent on the distance downstream of the dam, nearby topographic shading, and the time of year when they occur. Specifically, river temperatures become advection dominated under high flows, but will be controlled by a wide variety of surface heat fluxes during low flows. We test this hypothesis by adapting a dynamic routing and temperature modeling framework to capture the unique features of canyon-bound rivers and apply it to the highly regulated Colorado River in Grand Canyon. We analyze heat flux dynamics over a long simulation period (2000-2018) that includes typical daily fluctuations of flow, but also periods of both extended high and low flow experiments. While this paper does not explicitly evaluate climate change scenarios, quantifying the dominant heat transfer mechanisms provides a conceptual basis for inferring potential linkages between climate change and water temperatures in canyon-bound rivers. This modeling framework also provides the foundation for future work to investigate climate change projections and aquatic ecosystem implications.

2. Methods

2.1. Model formulation

In order to test our hypothesis about the key heat fluxes in canyon-bound rivers, we adapt a dynamic process-based routing and river temperature model to account for the influences of complex topography on river radiation balances. The foundational modeling framework, described by Buahin et al. (2019) and based on Neilson et al. (2010), includes various heat transfer and routing components that were developed and implemented within HydroCouple (Buahin & Horsburgh, 2018). The components included here are: EPA SWMM (Storm Water Management Model; Rossman, 2006) for dynamic wave hydraulic routing (solving the complete form of the St. Venant flow equations); the channel solute and heat transport (CSH) component for channel advection and dispersion, and sensible and latent heat fluxes; the radiative heat exchange (RHE) component used for shortwave and longwave radiation terms; the hyporheic transient storage (HTS) component used for sediment conduction; and the time series provider component to apply externally calculated scaling factors to select heat flux terms (i.e., spatial and temporal shading factors).

The CSH component uses the finite volume method to numerically approximate the 1D advection and dispersion heat transport equation:

$$\rho_w c_p \frac{\partial T_w}{\partial t} = \rho_w c_p \frac{\partial (v T_w)}{\partial x} + \rho_w c_p \frac{\partial}{\partial x}\left(D \frac{\partial T_w}{\partial x}\right) + \frac{\rho_w c_p}{V}(Q_{trib} T_{trib} + Q_{dist} T_{dist}) + \frac{J_{total}}{Y} \quad (1)$$

where T_w is the water temperature (°C), t is the time (s), v is the velocity of the water in the channel (m/s), x is the distance along the channel (m), D is longitudinal dispersion (m^2/s), ρ_w is the water density (kg/m^3), c_p is the specific heat capacity of water (J/kg/°C), Q_{trib} is the external flow from a tributary (m^3/s), Q_{dist} is the external distributed inflow or outflow (m^3/s), T_{trib} is the tributary temperature (°C), T_{dist} is the distributed flow temperature, J_{total} is the sum of all heat fluxes into and out of the river (W/m^2), V is the volume of the channel (m^3), and Y is the depth of water in the channel (m) that is calculated within the routing component as a function of channel shape and discharge. The J_{total} is calculated using the CSH, RHE, and HTS components and includes:

$$J_{total} = J_{sn,net} + J_{lw,net} + J_c + J_e + J_f + J_{sed} \quad (2)$$

where all heat fluxes are in W/m^2 and include net shortwave radiation ($J_{sn,net}$), net longwave radiation ($J_{lw,net}$), sensible heat (conduction and convection; J_c), latent heat (evaporation and

condensation; J_e), internal fluid shear friction (J_f), and sediment conduction (J_{sed}) (Figure S1). Air-water interface fluxes ($J_{sn,net}$, $J_{lw,net}$, J_c, and J_e) are a function of channel width which is determined by channel shape and discharge. In order to account for heat transfer processes associated with canyon-bound rivers, components $J_{sn,net}$, $J_{lw,net}$, and J_f were adapted from the original HydroCouple formulation and are described in detail below. Components J_e, J_c, and J_{sed} were not altered from the original formulation as described within Buahin et al. (2019).

2.2. Model adaptations

2.2.1. Radiation balance

Due to the attenuating, diffusive, and reflective effects of varying topography and river orientation on the net shortwave radiation received at the river surface ($J_{sn,net}$), it is necessary to account for the individual components of this radiation in canyon-bound systems at higher spatial and temporal resolution. Shortwave radiation was estimated as the sum of three individual terms (Figure 1): direct shortwave ($J_{sn,dir}$), diffuse shortwave ($J_{sn,diff}$), and land-reflected shortwave radiation ($J_{sn,refl}$; Eqn. 3).

$$J_{sn,net} = J_{sn,dir} + J_{sn,diff} + J_{sn,refl} \quad (3)$$

Process-based models commonly only consider longwave radiation coming from the atmosphere (J_{an}) and from the water (J_{br}). However, canyon-bound rivers are often adjacent to rock walls that can absorb radiation and re-emit longwave radiation. To account for this re-emitted radiation, the term J_{rock} was included in the longwave radiation balance (Figure 1). Therefore, the net longwave radiation balance is calculated as:

$$J_{lw,net} = J_{an} + J_{rock} - J_{br} \quad (4)$$

2.2.1.1. Shortwave radiation

Measurements of shortwave radiation within canyon-bound rivers are uncommon because these locations are often remote and difficult to access. Furthermore, the complex topography near any monitoring locations within canyons results in observations that are highly site-specific due to local shading dynamics. This makes it unrealistic to apply observations to river segments outside of the location where the observations were made. Therefore, in order to have realistic estimates of shortwave radiation reaching canyon-bound river surfaces, individual shortwave radiation terms ($J_{sn,dir}$, $J_{sn,diff}$, $J_{sn,refl}$) were estimated for specific river locations by scaling measured shortwave radiation ($J_{sn,meas}$) outside of the canyon. We do this by assuming that shortwave radiation measurements taken outside of the canyon are free from significant obstructions that would shade or influence observations via reflection from nearby features (e.g., canyon walls). Therefore, $J_{sn,meas}$ values represent:

$$J_{sn,meas} = \hat{J}_{sn,dir} + \hat{J}_{sn,diff} \quad (5)$$

where $\hat{J}$ denotes estimates of shortwave radiation on a horizontal surface (e.g., above the canyon). Note that since we assumed that $\hat{J}_{sn,refl} = 0$ for measurements outside of the canyon, this term was omitted from Eqn. 5.

Direct and diffuse components of $J_{sn,meas}$ can be separated out through the application of empirical correlation equations (Dervishi & Mahdavi, 2012). Because the relationship between these shortwave radiation components varies globally as a function of atmospheric characteristics, several models have been developed to fit site-specific observations (e.g., Erbs et al., 1982; Lam & Li, 1996; Orgill & Hollands, 1977). Each of these models result in a correlation equation (Text S1) that predicts the fraction of diffuse radiation (k_d) as a function

of the ratio between $J_{sn,meas}$ and modeled extraterrestrial radiation ($J_{sn,mod}$), known as the clearness index or clear sky index (k_t; Eqn. 6):

$$k_t = J_{sn,meas}/J_{sn,mod} \times \cos\theta \quad (6)$$

where θ is the solar zenith angle and values of k_t range between 0 and 1 with a value of 1 indicating clear sky. In this paper, $J_{sn,mod}$ was estimated using the Modular Distributed Watershed Educational Toolbox (MOD-WET; Huning & Margulis, 2015) functions in MATLAB. These functions calculate solar coordinates and top-of-atmosphere shortwave radiation as a function of geographical latitude and time. Applying k_t to the correlation equations results in an estimate of k_d above the canyon, such that

$$\hat{J}_{sn,diff} = J_{sn,meas}(k_d) \quad (7)$$

The $\hat{J}_{sn,dir}$ component is then calculated from Eqn. 5 via subtraction.

Direct shortwave radiation within a canyon. When trying to understand temperature dynamics in deep canyon settings over large spatial and temporal model domains, spatiotemporal shading information is needed to account for the variability in direct shortwave radiation reaching the water surface during different times of the year. A model for predicting shade in a canyon-bound setting, specifically Glen and Grand Canyon, was previously developed (Yard et al., 2005). However, this model predicts the photosynthetic photon flux density at the water surface, which is the visible light in the shortwave radiation spectrum (i.e., 400 nm – 700 nm). In order to get the complete estimate of shortwave radiation (~285 nm – 3000 nm), we developed an algorithm to compute topographic shade factors (S_f) over space and time following the methods of Yard et al. (2005; Text S2). These factors were calculated at regularly spaced increments along the river centerline and averaged over each respective model cell (c) to get $S_{f,c}$. $S_{f,c}$ is applied to the time variable direct shortwave radiation outside of the canyon ($\hat{J}_{sn,dir}$) to estimate the direct shortwave radiation reaching the water surface at each c:

$$J_{sn,dir,c} = (S_{f,c})\hat{J}_{sn,dir} \quad (8)$$

Diffuse shortwave radiation within a canyon. Diffuse radiation incident at the water surface is reduced by the fraction of the overlying visible hemisphere, referred to as the sky view factor (SV_f). SV_f can be calculated at specific coordinates along the river following the formulation from Dozier and Frew (1990). For these calculations only, we assume that the slope of the river could be approximated as zero to simplify the equation to:

$$SV_f = \frac{1}{2}\sum_{\Phi_j=1}^{360} sin^2\,(90 - \Psi_{E,\Phi}) \quad (9)$$

where Φ is the azimuth angle and $\Psi_{E,\Phi}$ is the elevation angle in the Φ direction (Figure 1). In this application, SV_f was calculated at regularly spaced increments along the river centerline and averaged over each respective c to get $SV_{f,c}$. The diffuse shortwave radiation reaching the water surface of each model cell over time is then calculated as:

$$J_{sn,diff,c} = (SV_{f,c})\hat{J}_{sn,diff} \quad (10)$$

Land-reflected shortwave radiation within a canyon. Land-reflected radiation is the combination of both direct radiation and diffuse radiation incident on the water surface which has been reflected off the surrounding terrain. This source of shortwave radiation can become

important in deep valleys when considering an entire year, but is generally small compared to the direct and diffuse components (Chen et al., 2006). While it is often neglected in river temperature modeling, for land surface energy budgets in deep mountain valleys, measured reflected shortwave radiation has been shown to be 14 to 21% of the incoming shortwave radiation (Matzinger et al., 2003; Whiteman et al., 1989). Due to rock walls being adjacent to many canyon-bound rivers, it is presumed that a portion of the reflected shortwave radiation makes it to the water surface. We included reflected shortwave radiation, calculating it following Gates (1980) as:

$$J_{sn,refl,c} = \alpha_{land}(1 - SV_{f,c}) \times (\hat{J}_{sn,dir} + \hat{J}_{sn,diff}) \quad (11)$$

where α_{land} is the albedo of the surrounding terrain. This approach does not account for conditions where only a fraction of the terrain is illuminated by $\hat{J}_{sn,dir}$, but instead assumes that $J_{sn,refl}$ is isotropic. Because $J_{sn,refl}$ is reportedly small (Chen et al., 2006), the complex process of modeling the anisotropic nature of $J_{sn,refl}$ that involves computing multiple reflections from all viewable terrain cells was not considered.

2.2.1.2. Longwave radiation

Rock longwave radiation. Heat emitted from rock as longwave radiation was estimated following the Stefan-Boltzmann Law (Chapra, 1997). However, because the intensity of longwave radiation quickly attenuates as you move away from its source, only rock features adjacent to the river are expected to contribute significant amounts of heat to the river. In order to account for this effect, we recomputed the SV_f only considering terrain within 5 m from the river's edge ($SV_{f,5}$). Following Eqn. 9, $SV_{f,5}$ were calculated at specific coordinates by replacing elevation angles (Ψ_E) with land re-emittance angles (Ψ_L), where Ψ_L is defined as the largest angle between river center and the adjacent terrain within a distance of 5 m from the river banks (Figure 1). The $SV_{f,5}$ were averaged over space for each c to get $SV_{f,c,5}$. J_{rock} was then computed as:

$$J_{rock,c} = (1 - SV_{f,c,5})(\varepsilon_{lc}\, \sigma\, T_{rock}^4) \quad (12)$$

where σ is the Stefan-Boltzmann constant ($W/m^2/K^4$) and $\mathcal{E}_{lc}$ is the emissivity of the land. T_{rock} is the rock temperature (K) and was assumed to be the same as the air temperature (T_{air}). This assumption was consistent with other studies that estimated longwave radiation from both terrain and vegetation (Benyahya et al., 2012; Caissie, 2016; MacDonald et al., 2014). It is considered to be an underestimate of temperature for terrain sources because direct shortwave radiation can elevate rock surface temperatures approximately 10-25 °C higher than the ambient air temperature, while shaded surfaces will be equal to or slightly cooler than the ambient air temperature due to convective or evaporative fluxes (Gates, 1980; Larson et al., 2000).

Atmospheric longwave radiation. Heat emitted from the atmosphere as longwave radiation is obstructed by surrounding topography, reducing the amount that is received at the water surface. To account for this, atmospheric longwave radiation was scaled by the sky view factor that considered terrain greater than 5 m from the shoreline. Therefore, the formulation of J_{an} is:

$$J_{an,c} = SV_{f,c,5}(\varepsilon_{atm}\, \sigma\, T_{air}^4)(1 - R_L) \quad (13)$$

where $\mathcal{E}_{atm}$ is the emissivity of the atmosphere and R_L is the reflection coefficient.

2.2.2. Internal fluid shear friction

Heat generated by friction is typically small in rivers, but can be a significant source of heat in steep streams (Meier et al., 2003; Theurer et al., 1984) or streams with relatively high discharge, both of which can be present in canyon-bound rivers or streams. Heat generated in this process is related to the potential energy lost from the change in elevation, resulting in friction and turbulent energy dissipation. Following the formulation by Theurer et al. (1984), internal fluid shear friction was added to the CSH component and is a function of flow, bed slope, and channel width (Text S3).

2.3. Model application

2.3.1. Study Site: The Colorado River in the Grand Canyon

The Colorado River flows for approximately 800 km through the uplifted landscape of the southern Colorado Plateau, including 450 km of the Grand Canyon. Within Grand Canyon, the most downstream 65 km of the river is inundated by Lake Mead. Immediately upstream from Grand Canyon, the river is impounded by Glen Canyon Dam forming Lake Powell (Figure 2). The river in Grand Canyon is organized in a series of steps, with steep, turbulent rapids, and flat intervening sections (Magirl et al., 2005). Surrounding the river, the terrain is topographically complex with an average canyon depth of 1,200 m and average width of 1,600 m which limits the amount of direct shortwave radiation received at the water surface (Yard et al., 2005). As the Colorado River flows through this region, it often changes orientation, resulting in dynamic shade patterns that are highly variable over time from one river kilometer to the next. In many sections of the canyon, the river adjoins bedrock features which complicate the radiation balance by re-emitting longwave radiation to the water surface (Stanitski-Martin, 1996). The geology is comprised of nearly 40 major sedimentary rock layers including limestone, sandstone, shale, and metamorphic schist and granite intrusions (Karlstrom et al., 2012). Many seeps and springs emerge from the limestone layers that are karst (Fitzgerald, 1996; Goings, 1985; Zukosky, 1995), feeding several perennial tributaries that combined, contribute an average discharge of approximately 30.4 m^3/s to the Grand Canyon on an annual basis (Figure S2).

Comprehensive information about the management of Glen Canyon Dam and the effects it has had on flow regimes, water quality, and aquatic ecology in the downstream Colorado River can be found in Gloss et al. (2005) and U.S. Bureau of Reclamation (2012). An exhaustive review of this material is outside the scope of this paper, however, a brief summary of river temperature characteristics, data collection programs, and modeling efforts is provided in Text S4. While these studies are major contributions to our understanding of hydrology and river temperature within Grand Canyon, the actual mechanisms controlling temperatures in the Colorado River have yet to be identified and quantified. The work presented here seeks to build on the considerable body of literature that already exists for the Colorado River while also building our understanding of river temperature controls in flow regulated canyon-bound rivers.

2.3.2. Model domain, simulation period and forcing data

To understand the dominant processes controlling water temperatures in Grand Canyon, we modeled flow and temperature for a 362 km section and 18-year period (Jan. 1, 2000 to Jan. 1, 2018) at approximately a 1 km spatial and hourly temporal resolution. This simulation period was largely dictated by the availability of sub-daily (15-20 minute) temperature data at the USGS gage at Lees Ferry (*USGS 09380000 Colorado River at Lees Ferry, AZ*) that was used as the upstream boundary condition in the model (Table S1). This gaging station is the oldest main channel gage that has measurements of both discharge (Q_{BC})

and temperature (T_{BC}) downstream from Glen Canyon Dam (Figure 2). The most downstream gage that measures discharge and temperature became the downstream modeling domain boundary and is located above Diamond Creek (Table S1), approximately 362 km downstream of Lees Ferry. Four additional main channel discharge and temperature measurement sites (RM30, RM61, RM88, RM167) located between Lees Ferry and Diamond Creek, at the transition of geomorphically distinct river segments (labeled segments in Figure 2) were used for model development, hydraulic routing calibration, and evaluation of the river temperature model. The nomenclature for defining river segments between these gages was adopted from Melis (2011). When reporting locations within our results, we use the river mile (RM) convention that is well established for the Grand Canyon where RM zero is located at Lees Ferry and downstream river distances are positive while upstream river distances are negative.

For hydraulic routing (using the SWMM component), channel geometry data between Lees Ferry (RM0) and Diamond Creek (RM225) were obtained from a subset of 2,680 cross-sections delineated from LiDAR by Magirl et al. (2008) and aggregated to the selected 1 km model cell size. Model cells representing locations of tributary inflows or main channel gaging stations were shortened to approximately 200 m and centered around the tributary inflow or gage in order to better represent local conditions. All other components used for the river temperature modeling (i.e., CSH, RHE, and HTS) use identical discretization as the SWMM component.

Channel roughness was calibrated for 2013 and 2014 on a segment-by-segment basis (Figure 2) by sequentially incrementing Manning's roughness values. Calendar years 2013 and 2014 were chosen to perform routing calibration because they have flow distributions that are representative of the entire simulation period. In an effort to capture the extreme flow variability, SWMM was run for sequential 2-week periods over the 2 years with roughness values being varied between 0.02 and 0.05 in 0.001 increments. The Manning's roughness values that minimized the root mean square error (RMSE) for each 2-week period were averaged to produce a single Manning's roughness value for each river segment. These estimated roughness values (Table S2) are comparable to those reported by Magirl et al. (2008). Previous routing models for the Colorado River in Grand Canyon suggest that roughness is stage dependent (Graf, 1995; Magirl et al., 2008; Wiele & Smith, 1996), however, given our ability to capture the highly variable flow conditions that occurred over the simulation period and the limited structure in modeled discharge residuals, constant roughness values were applied.

2.3.2.1. Tributary data

Gaged tributaries within the model domain were directly accounted for in the routing and temperature modeling components (Figure 2; Table S1). These tributary gages are located close enough to the Colorado River confluence such that travel time between the gage and confluence were not considered. Most of these tributaries have periods of missing data during the simulation period. Large gaps in the flow record (i.e., greater than 2 days) were filled by assuming flows during that period were equal to the annual median flow. However, in the Little Colorado River (LCR), the largest tributary within Grand Canyon, flow is almost entirely from Blue Springs (Fitzgerald, 1996) and required this location to be handled differently. To account for periods with missing data at the LCR gage near the confluence (*USGS 09402300*), the gage upstream of Blue Springs (*USGS 09402000 Little Colorado River near Cameron, AZ)* was also used by adding median flow estimates to the upstream gage measurements and applying a constant time offset that represents the approximate travel time between the upstream gage and confluence. The travel time was determined by comparing hydrographs from the two gaging stations. Similarly, temperature gaps were filled

such that the heat contribution from tributaries could be better represented during these times. This was done by first calculating the monthly average temperature from the available data. In order to capture the diurnal pattern of temperatures, hourly variability for each month was also calculated. The hourly variability for each month was then added to the monthly average temperatures in order to get a representative temperature series. To compare the relative heat contributions from the tributaries (J_{trib}) to the other heat fluxes in equation 2, the apparent sensible heat flux from the tributaries were calculated following Kurylyk et al. (2016; Text S5; Eqn. S6).

2.3.2.2. Distributed flows

Monthly differences in streamflow volume between gaging stations, accounting for gaged tributaries, were computed to close the mass balance and applied to the model as Q_{dist}. A monthly time step was chosen so that travel times between gages and the timing of flash floods from ungaged streams would not greatly influence the volume estimates. This resulted in monthly estimates of Q_{dist} (both positive and negative) for each segment. Because of the uncertainty surrounding the source of gage differences (tributary inflows, groundwater inflows or outflows, or gage error), these estimates were applied evenly over each model segment with a constant temperature. The mean annual air temperature from within Grand Canyon (Table S3) was used as an approximate temperature for all distributed inflows (T_{dist}. Eqn. S7). Similar to the tributary heat contributions, the apparent sensible heat flux from distributed inflows (J_{dist}) was calculated following Kurylyk et al. (2016; Text S5) for comparison purposes.

2.3.2.3. Meteorological data

Historical climate data used to estimate air-water surface interface heat fluxes were obtained from Page, AZ airport using University of Utah's MesoWest Database (herein referred to as MesoWest; https://mesowest.utah.edu; Figure 2). These data include air temperature, wind speed, and relative humidity. Data from Phantom Ranch near RM88 (Table S3) was not directly used in the model because sub-daily data does not exist for the entire simulation period. Therefore, air temperature data from Page, AZ was regressed to measurements made at Phantom Ranch at hourly intervals. This allowed the use of the longer-term Page, AZ air temperature data while representing the differences in air temperature magnitude and patterns in Grand Canyon (Figure S3). Similarly, air temperature, wind speed, and relative humidity data from within the canyon were available from the GCMRC (Caster et al., 2014), but again, they do not cover the full simulation period. The air temperature data from GCMRC and Phantom Ranch were, however, used to estimate a mean annual air temperature of 20 °C and to determine how well the regressed air temperature represents other sections of Grand Canyon (Table S3). While relative humidity and wind speed within the canyon will be significantly different than those from Page, AZ, the values will be highly variable over space and time due to microclimates created within the canyon (Stanitski-Martin, 1996). To avoid inconsistent forcing data for the simulation period and arbitrary assumptions regarding the applicability of site-specific data collected within the canyon, we applied the Page, AZ regressed air temperature and Page, AZ wind and relatively humidity data uniformly to the entire study area.

Shortwave radiation data measured at wildland fire remote automated weather stations (RAWS) dispersed around the Grand Canyon region were obtained from MesoWest (Figure 2; Table S4). Shortwave radiation measurements at these sites were aggregated into an hourly median time series and used in the model as a single time series ($J_{sn,meas}$; Figure S4). It was assumed that these sites were free from vegetation or topographic shading so that they could be disaggregated into the various shortwave radiation components as discussed earlier.

2.3.4. Sediment conduction

For sediment conduction (Figure S1), the depth of the shallow sediment layer (Y_{sed}) was assumed to be 0.5 m and the depth to the ground boundary layer (Y_{gr}) was assumed to be 1 m. The mean annual air temperature was used for the lower boundary condition (T_{gr}).

2.3.5. Radiation balance in Grand Canyon

2.3.5.1. Shortwave radiation

Direct Shortwave Radiation. Topographic shade factors, S_f, were calculated every 100 m along the river centerline following the algorithm described in Text S2 and averaged over each corresponding model cell before being applied to the direct shortwave radiation term (Eqn. 8).

Diffuse Shortwave Radiation. Yard et al. (2005) showed that diffuse radiation made up a significant portion of the annual shortwave radiation budget in Grand Canyon, with some sites receiving no direct shortwave radiation for 194 days. In order to determine which of the models presented by Dervishi and Mahdavi (2012) is best for representing diffuse radiation conditions near Grand Canyon, measurements of shortwave radiation were collected during a 1-month period (May 15 – Jun 27, 2019) in the LCR drainage approximately 6 km upstream from the main channel Colorado River. This site was chosen because of its deep canyon topography and geology that is similar to the Grand Canyon. Two Hukseflux LP02 (Manorville, NY) pyranometers (spectral range = 285-3000 nm) were deployed on the east and west banks, approximately 30 m from the river, in a south-north orientated river segment. These sensors were set up to sample every 5 minutes and record the average shortwave radiation every 15 minutes. This configuration was chosen to identify the differences in magnitude between direct and diffuse shortwave radiation and to capture the timing of morning and evening shade dynamics for comparison against the shade algorithm.

Similar to direct shortwave radiation, following Eqn. 9, SV_f was calculated every 100 m along the river centerline and averaged over each model cell in order to determine the amount of diffuse radiation at the water surface (Eqn. 10). Given that the river has an average gradient of 0.0015 (Wiele & Smith, 1996) and is comprised of long flat sections separated by short steep rapids (Magirl et al., 2005), our assumption of a zero slope for this calculation was reasonable for most of the canyon.

Land-Reflected Shortwave Radiation. In Grand Canyon, measurements and regional estimates of land surface albedo suggest approximately 20% reflectance (Stanitski-Martin, 1996). However, the actual portion reflected toward the river is likely small given the complex nature and orientation of the landscape relative to the water surface. Therefore, we applied a constant α_{land} of 1% such that $J_{sn,refl}$ is a very conservative estimate.

2.3.5.2. Longwave radiation

Rock longwave radiation. J_{rock} was estimated using land re-emittance angles computed from terrain within 5 m from the modeled shoreline at flows of approximately 878 m^3/s (Magirl et al., 2008). This was handled by clipping a digital elevation model (DEM) to a 5-m buffer of the river shoreline and computing $SV_{f,5}$ every 100 m along the river centerline and averaging them for each corresponding model cell. An $\mathcal{E}_{lc}$ of 0.9 was chosen for all terrain based off of reported values for limestone and sandstone surfaces (Eqn. 12; Brewster, 1992).

2.3.6. Model scenarios

2.3.6.1. Simplified radiation scheme

Shading in canyon-bound rivers has previously been handled using seasonal and reach specific shading factors (e.g., Carron, 2000). In order to understand and demonstrate the importance of a complex radiation balance in canyon-bound rivers, we applied a simplified shading scheme to produce seasonally averaged shade factors for each river segment (Figure 2) that was used to scale shortwave radiation values applied in the temperature model. Seasons were divided into Winter (Dec, Jan., and Feb.), Spring (Mar., Apr., and May), Summer (Jun., Jul., and Aug.) and Fall (Sep., Oct., and Nov.). J_{rock} was not accounted for in these simulations, resulting in J_{br} and J_{an} being the only longwave radiation sources. This model is herein referred to as the "simplified" model, while the model using the complex radiation balance described above is referred to as the "detailed" model.

2.3.6.2. Long term model simulation

An 18-year simulation period for the entire domain (RM0 to RM225) was used to determine the large scale spatial and temporal differences between the simplified and detailed radiation schemes. More broadly, this space and time domain also was used to determine whether accurate predictions of river temperature could be made over long time ranges with highly variable flow and weather conditions over a large spatial extent. The long simulation period also allowed us to test assumptions of constant channel geometries and hydraulic roughness coefficients, which is important when modeling future climate change and/or hydrologic conditions. Additionally, the long-term simulation was used to determine if the assumptions applied to meteorological input data were appropriate for calculating heat fluxes over a large range of conditions. Model performance was evaluated by calculating RMSE and Nash-Sutcliffe Efficiency (NSE) for discharge and temperature at each gaging stations over the entire simulation period by matching model outputs (hourly) to historical observations with a tolerance of ±5 minutes. Histograms of the model residuals were also created to determine whether positive or negative prediction bias was present over time and space.

2.3.6.3. High and low flow comparison

Investigating differences between the simplified and detailed models under different flow regimes can help determine when and where detailed radiation information becomes important for predicting instream temperatures. We focused comparison on a low flow period that occurred during summer 2000 and a high flow period that occurred during the summer of 2011. During the low flow period releases from Lake Powell were held constant at approximately 226 m^3/s between June and September as part of the Low Summer Steady Flow (LSSF) experiment . During the high flow period discharge was held steady at approximately 700 m^3/s between July and September in order to satisfy water storage agreements via so-called "equalization flows" (an interim operating criteria to equalize storage between Lake Powell and downstream Lake Mead; U.S. Department of the Interior, 2007).

2.3.6.4. Heat flux analysis

Using the results from the detailed long-term model simulation we were able to investigate the dominant heat fluxes controlling river temperatures over space and time in this canyon-bound river. Minimum, mean, and maximum heat flux statistics were calculated for each individual heat flux over the model simulation period and domain. Statistics for the relative contribution (%) were calculated from absolute values for each heat flux over space and time divided by the sum of absolute values for all heat fluxes over space and time. The

absolute percent contributions of heat fluxes were also evaluated at individual river segment and month scales to identify if dominant mechanisms changed over the model domain or over the calendar year.

2.3.6.5. Sensitivity analysis

To quantify the sensitivity of individual heat fluxes in the detailed long-term model simulation to perturbations of input time series data, we altered input meteorological observations (shortwave radiation, wind speed, relative humidity), Q_{BC}, Q_{dist} and T_{dist} arbitrarily by ± 10% to account for measurement uncertainty and spatial representativeness of measurements. Rock temperature (estimated from air temperature) was altered independently from air temperature by ± 10%. We also varied T_{BC} by ± 0.2 °C to account for sensor accuracy. Air temperature was perturbed ± 1.0 °C to account for spatial uncertainty in the regression applied between Page and Phantom Ranch (Figure S3; Table S3). The residual between the detailed model and each perturbation was then evaluated to determine if temperature predictions changed significantly compared to the detailed model. This approach can highlight which data are most important and provide insights into how the system may respond to changes in climate, hydrology, or upstream reservoir release temperatures.

3. Results

3.1. Radiation balance

Measurements of shortwave radiation in the LCR ($J_{sn,LCR}$) revealed the timing of shading dynamics and the magnitude of shortwave radiation within the canyon. On a clear-sky day, the timing of direct incidence and shade at the bottom of the canyon was obvious from the data collected (Figure 3). For example, on June 19, 2019, our measurement site remained in the shade till 9:30 AM and went back into the shade by 3:30 PM. Our shading model captures this timing within 15 minutes (Figure 3). Discrepancy in the timing is likely due to the chosen sampling frequency used in the model and data collection.

Using the correlation equations presented by Dervishi and Mahdavi (2012), we disaggregated $J_{sn,meas}$ into above canyon estimates of $\hat{J}_{sn,dir}$ and $\hat{J}_{sn,diff}$ (i.e., Eqn. 5, 6, 7), that were used to determine the individual components $J_{sn,dir}$, $J_{sn,diff}$, and $J_{sn,refl}$ at the water surface (i.e., Eqn. 8, 10, 11), which sum to get $J_{sn,net}$ (i.e., Eqn 3). Comparison of predicted $J_{sn,net}$ to $J_{sn,LCR}$ measurements found that the formulation by Erbs et al. (1982; Text S1) produced the lowest RMSE over the entire sampling period. For $J_{sn,net}$ during a clear sky day (e.g., Jun. 19, 2019), the model yielded a RMSE of 52.3 W/m^2 (Figure 3). Over the entire data collection period (43 days), the RMSE for $J_{sn,net}$ is higher (132.8 W/m^2) because estimates of shortwave radiation were less accurate during local overcast conditions. This result is not a surprise given that the $J_{sn,net}$ value is estimated from $J_{sn,meas}$, which is aggregated from multiple locations spanning the entire Grand Canyon region. Regardless, the timing of shade predicted by our algorithm agrees with the timing observed in the LCR and the magnitude of diffuse radiation in the morning and evening matches what was measured (Figure 3). These results illustrate that our method for capturing the timing of shading and the magnitude of diffuse shortwave radiation is appropriate.

3.2. Long-term model results

Modeled discharge. Long-term model results for discharge indicate accurate model predictions given the long simulation period, highly variable flow conditions, and large spatial extent of the model (Figure S5). The histogram of residuals (observed minus modeled) show that we do not have a positive or negative bias in flows at any of the gaging stations

indicating that our approach to closing the flow balance is reasonable. As expected, flow routing prediction errors increase downstream due to the propagation of errors throughout the entire model domain. Overall, the error at the most downstream model element is less than 3% of the average flow. Because there is no apparent temporal drift in the accuracy of the routing predictions, our assumptions of constant channel roughness coefficients and channel geometry are reasonable for representing the hydraulics over long periods of time and highly variable flow conditions.

Modeled temperature. Long-term model results using the simplified and detailed radiation schemes for temperature predictions at the five main channel gaging stations indicate that high resolution shading dynamics and rock longwave radiation significantly improves model predictions, particularly over large spatial domains (Figure 4; Figure S6). Histograms of the residuals for the detailed simulation are slightly positive with peaks around 0.2 °C for all sites except for RM225, which has a slightly higher bias of approximately 0.5 °C. Bias in the simple model was higher at all sites, with RM225 having a histogram peak around 1.5 °C. These positive residuals indicate a persistent underestimation of temperatures in each river segment. Similar to our discharge results, prediction errors increase downstream as error from upstream segments propagate to downstream segments.

Spatial and temporal model performance. Monthly model residuals reveal that there are also temporal differences between the simple and detailed radiation schemes (Figure S7). While the detailed model produces underestimates for many months and locations, overestimates do occur in summer months with June being the greatest. During this period, overestimates are increasing downstream up to RM88, but then decrease as you move further downstream. This indicates that local attributes within particular river segments may be influencing river temperature that are not fully captured in the detailed model (e.g., rock longwave radiation or local meteorological conditions). Underestimates of temperature in the detailed model are greatest during late fall and early winter months for all sites. Water temperatures at RM225 have the highest residuals and are underestimated in all months, but median residuals are below 1 °C (Figure S7). Residuals from the simple simulation have higher variability over both space and time. The simple model produces significantly lower temperature predictions for nearly all months and locations, with greatest underestimates occurring during late spring, summer, and early fall months, and at the downstream river gages.

3.3. High flow and low flow period model results

Discharges during the summer of 2000 were three times lower than in 2011, with flows during these periods averaging 235 m^3/s and 700 m^3/s, respectively (Figure 5). While these significantly different flow regimes alter the volume of water that must be heated or cooled, prediction errors from the detailed model were similar for the two periods at RM61 and RM88, with differences in RMSE within tenths of a degree (Figure 5). Larger differences in the detailed model predictions arise downstream of RM88. During the low flow period the RMSE at RM167 jumped to 1.25 °C while the RMSE at RM167 during high flows decreased to 0.47 °C. Temperature data at RM225 is limited to Aug. 6 – Aug. 20 in 2000, and therefore, we do not report an RMSE during this period. However, the RMSE at RM225 during high flows were lower again at 0.34 °C (not shown in Figure 5). The simple model had worse, but reasonable results during the high flow period at all sites. During the low flow period the simple model significantly underestimated temperatures at all sites.

3.4. Dominant heat fluxes

3.4.1. All modeled external heat fluxes over time and space

For the detailed simulation, 9 of the 12 evaluated heat fluxes made up a significant portion (> 40%) of the of the total heat budget at any given time over the model domain (Table 1). We found that $J_{lw,net}$ (incoming minus outgoing) was on average negative, however, $J_{lw,net}$ switched to a positive flux at times when J_{rock} was relatively high. Sensible (J_c) and latent (J_e) heat fluxes were highly variable and were both positive and negative. High sensible heat fluxes were largely due to periods of high wind speed coinciding with high air temperature relative to water temperature (> 20 °C difference), which is common due to cold, hypolimnetic releases from Glen Canyon Dam coinciding with warm summer air temperatures. Positive and negative extremes in latent heat values, which correspond to greater condensation or evaporation, respectively, occurred when there were relatively large differences between air temperature and water temperature (> 20 °C) coinciding with high relative humidity (~78%) or low relative humidity (~4%), respectively. Surprisingly, friction had the largest maximum heat flux magnitude of 2047 W/m^2, which occurred under a high flow experiment on Nov. 12, 2012, where flows exceeded 1250 m^3/s in a model cell that has an approximate slope of 0.7% and width of 41 m at this discharge. However, the average contribution for J_f was modest and similar to sensible heat. Lateral heat fluxes provided by tributaries and distributed inflows were both positive and negative. Negative lateral heat fluxes occurred when river temperature was warmer than the temperature of the source or when distributed flows (Q_{dist}) were negative. J_{trib} had the second largest maximum heat flux magnitude of 1475 W/m^2, which occurred during a flash flood event.

The high maximum relative contribution from most of the heat fluxes indicates that mechanisms for heating and cooling are highly dynamic over both space and time (Table 1). This is further illustrated by the change in relative contribution of heat fluxes for the five model segments during each season of the year averaged over the entire simulation period (Figure 6). Relative contributions from $J_{sn,net}$ are lowest during the winter and increase in the summer, corresponding with patterns in solar zenith angles throughout the year. $J_{sn,net}$ contributions are smallest in East Central Grand Canyon during winter, which is due to a predominant East – West orientation and particularly high elevation angles when compared to other river segments (Figure S8). $J_{lw,net}$ contributions are highest in winter, when other heat fluxes are small, and lowest in summer, when J_e and J_c become more dominant. J_{sed} contributions do not vary significantly over space or time. The relative contributions from J_{lat} (sum of J_{trib} and J_{dist}) are highly variable over space and time, where again, the largest contributions corresponded with flash floods.

3.4.2. Fluxes during high and low flows

Between high and low flow periods the relative contributions were relatively similar for most heat fluxes (Figure S9). Friction heat (J_f) had the largest change in percent contribution by more than doubling between these two periods (~10% during low flows and ~21% during high flows) due to the nearly three-fold difference in discharge. $J_{sn,net}$ remained the dominant heat flux under high and low flow conditions. The relative contribution of $J_{lw,net}$, J_e, and J_c decreased during the high flow period even though the surface area of the river increased 17%. While width increased under high flows, it was relatively small compared to the increase in volume.

3.5. Sensitivity analysis

Temperature predictions from the detailed model were compared to subsequent simulations where input data were perturbed to determine the sensitivity of forcing data on

temperatures through space and time (Figure 7; Figure S10). Positive and negative residuals generally increased further downstream for all perturbations except for changes to T_{BC}, which on average has lowest temperature residuals at RM225, regardless of season. Positive perturbations of input data often resulted in negative temperature residuals (predictions greater than those in the detailed model) except for Q_{BC} and wind speed, which resulted in positive temperature residuals during most seasons. At the most upstream location chosen for comparison (RM30), the perturbation in T_{BC} (± 0.2 °C) creates the greatest residual between the detailed model than any other perturbation. This suggests that water in the first 30 miles is moving through this segment at a rate fast enough (approximately 7 hours) to not be influenced by climate variables and the model is mostly propagating T_{BC} for any time of year. At RM88, perturbation of T_{BC} still produces the largest median residual between the detailed model and any other perturbation during winter and fall. However, perturbations of $J_{sn,net}$, T_{air}, Q_{BC}, and T_{BC} have residuals of comparable magnitude during spring and summer. Water travels from Lees Ferry to RM88 in approximately 20 hours, which allows more time for external heat sources and sinks to influence river temperatures. Further downstream at RM225, the influence of T_{BC} becomes less pronounced and the perturbations of Q_{BC} and climate variables have even higher magnitude residuals, with $J_{sn,net}$, T_{air}, and Q_{BC} perturbations creating the largest deviations from the detailed model temperature predictions during summer. At each location and during all seasons Q_{BC} has the most variability as indicated by the broad distribution of residuals. Perturbations in wind speed, T_{rock}, Q_{dist}, and T_{dist} result in only minor differences from the detailed model suggesting that warming or cooling of the river is less sensitive to these variables. Q_{trib} (not shown) was also perturbed by ±10% but was found to be less influential on river temperatures than the variables show here.

Sensitivity analyses constrained to the high and low flow periods show that river temperatures during high flows are sensitive to T_{BC} throughout the entire canyon (Figure S11). Under high flows the influence of other inputs is relatively small at RM30, but the role of $J_{sn,net}$, T_{air}, and Q_{BC} increase downstream, creating the largest temperature residuals at RM225. River temperatures during low flows are most sensitive to perturbations of T_{BC} at RM30, but that sensitivity is reduced downstream and $J_{sn,net}$, T_{air}, Q_{BC}, and relative humidity become more sensitive. Between RM30 and RM225, all inputs create higher magnitude residuals during the low flow period when compared to the high flow period, with the exception of T_{BC} at RM225. This indicates that temperature of water released from the dam is altered more during low flow and the rate of change is controlled by a wide variety of heat fluxes.

4. Discussion

Consistent with our hypothesis, the results from this work show that the dominant heat fluxes in canyon-bound rivers are highly dynamic over space and time. As with other systems, shortwave radiation is the dominant heat flux when considering the entire simulation period and model domain. However, the influence of typically smaller air-water heat fluxes become more important during fall and winter periods when portions of the river experience more shading and have limited direct shortwave radiation. Flow regulation is also a major control on river temperatures in the Colorado River, as pointed out by Anderson and Wright (2007). We expect other canyon-bound rivers to experience similar variability in dominant heat fluxes, but when and where these changes occur would be based on a combination of site-specific influences (e.g., variability in spatial orientation, flow, complexity of surrounding topography).

4.1. Radiation balance

Our approach to incorporating shade predicts the onset and departure of direct shortwave radiation within 15 minutes when compared with measured conditions in the LCR study area (Figure 3). This method is computationally simplistic, but estimates are completed at sufficiently high resolution to account for the spatial and temporal shading dynamics within Grand Canyon. While others have used similar approaches to predict shade in temperature models (Chen, et al., 1998b; Cox & Bolte, 2007), our method for determining elevation angles and the timing of shade is computationally similar to Yard et al. (2005; Text S2) with nearly identical predictions (Figure S12). However, the key difference between our approach and Yard et al. (2005) is our use of shortwave radiation from outside of the canyon to estimate the amount received at the water surface. Our results illustrate that accurate predictions of shade timing are critical for estimating direct shortwave radiation ($J_{sn,dir}$), and ultimately estimating river temperatures.

Diffuse shortwave radiation ($J_{sn,diff}$) is also an important component of the radiation balance (Table 1). While some river temperature models have partitioned shortwave radiation data, either as a fixed ratio (Rutherford et al., 1997; Westhoff et al., 2007) or using an approach similar to the one implemented here (Chen, et al., 1998b; Leach & Moore, 2010), applications rarely have access to measured data to evaluate the best empirical approach. Loinaz et al. (2013) is the only example found where measured diffuse shortwave radiation was directly applied in a model, however, this work provided no details as to how these measurements were made. Here, we found that having physical measurements to help us choose an appropriate correlation equation for partitioning $J_{sn,meas}$ to be important, especially since $J_{sn,diff}$ had a generally high maximum relative contribution of up to 32% at times (Table 1).

Reflected shortwave radiation ($J_{sn,refl}$) provides negligible amounts of heat to this large river. Our approach to estimating $J_{sn,refl}$ was relatively simple and we acknowledge the complexity in obtaining more detailed flux estimates. We anticipate the need for these advanced methods for narrower and lower flow canyon-bound streams.

Longwave radiation from the rock walls contributes a small amount of heat to most of the river in Grand Canyon. While never a major heat flux to the river, longwave radiation from rock walls increased during summer in the narrowest parts of Grand Canyon. Given that air temperature likely underestimates the actual temperature of the rock walls (Larson et al., 2000), and that rock temperatures likely lag behind the timing of air temperatures due to the significantly higher specific heat capacity, the J_{rock} estimates do not fully represent the diverse conditions within the canyon. Furthermore, view angle estimates computed from the center of the river, as opposed to calculating it from several points along a transect, could produce underestimates of $SV_{f,c,5}$. In some situations, there may also be a need to account for detailed longwave radiation from riparian vegetation.

4.2. Long term model results

The results from the 18-year simulation period and 362 km long model domain, demonstrate that a detailed radiation scheme is important when predicting over large spatial extents and different times of the year (Figure 4). The temperature RMSE for the detailed radiation model simulation over the entire period at RM225 is 0.93 °C, however, temperature predictions are underestimated most of the time. The persistent under prediction of temperature indicates a missing heat source within the model or a misrepresentation of the heat fluxes included. A main source of error may be due to changes in local meteorology within the canyon deviating from the meteorological conditions at Page, AZ (the source for relative humidity, wind speed) and potential errors in the regressed air temperatures (Table S3). This conclusion is supported by the sensitivity analysis, which shows that perturbations

in T_{air} causes some of the most significant residuals at RM225 for all periods (Figures 7 and S10). Inclusion of additional weather stations was considered, however, they were omitted to avoid inconsistent forcing data for the simulation period and arbitrary assumptions regarding the applicability of site-specific data to other areas within the canyon. Similarly, overestimation of temperatures in the upstream river segments during summer months, particularly in June (Figure S6), were potentially due in part to inaccurate estimates of shortwave radiation from aggregating all radiation measurements above the rim into a single time series. In other words, we are not accounting for longitudinal differences among sites and this influences the timing and magnitude of $J_{sn,meas}$ that is scaled within the model. To address these meteorological challenges, future modeling efforts should investigate the feasibility of alternative data sources (such as remote sensing or climate reanalysis products) for acquiring input meteorological variables and applying them over remote, topographically complex regions.

Lateral inflows from seeps, springs, or ungaged tributaries may also be adding more or less heat than anticipated. Between Lees Ferry and RM225 the river gains approximately 30.4 m^3/s annually, half of which is accounted for in the gaged record of tributaries, leaving 14.6 m^3/s (4% of the total annual flow) being contributed to the river from unknown sources (Figure S2). While we accounted for the additional flow from unknown sources within river segments as evenly distributed inflows at a constant water temperature of 20 °C, most of these flows likely come from small ungaged tributaries that have different thermal characteristics. Lateral inflow heat fluxes (Eqn. S5) make up 5% of heat exchange on average (Figure S9) but can be higher during different times and at different locations due to flash floods (Figure 6; Table 1). Therefore, a better understanding of seeps, springs, or ungaged tributaries and associated inflow temperatures may improve temperature predictions. Temperature prediction errors could also be rooted in our flow routing errors. The sensitivity analysis results show that by RM88 a 10% perturbation in flow could result in up to ± 0.5 °C change in temperature predictions relative to the detailed model run for most seasons (Figures 7 and S10). While our flow routing predictions are well within 10% of the observed flows, better routing may improve river temperature predictions.

Lastly, a few heat transfer mechanisms were intentionally omitted from this model, including groundwater exchanges, hyporheic exchange, and surface transient storage. While each of these processes likely occur to some degree, these were ultimately left out of the model because they were expected to be negligible based on findings in the literature or site-specific conditions (Text S6).

4.3. High flow and low flow periods

Our results from modeling high flow and low flow periods with a detailed radiation scheme agrees with the conclusions made by Anderson & Wright (2007), that the river temperatures are significantly influenced by the advection of heat during high flow periods. However, this work expands on previous river temperature modeling studies within Grand Canyon (Text S4) by evaluating the change in relative contribution from individual heat fluxes between different flow regimes. We found that the heat contribution from friction more than doubled under high flows, which had approximately three times more discharge than the low flow period. With the increase in flow, it would be expected that the surface area would also increase, allowing for greater contributions of air-water interface heat fluxes. However, the high flow period only resulted in a 17% increase of surface area when compared to the low flow period due to the confining channel margins. Poor predictions at RM167 for the low flow period (Figure 5) were likely due to limited information about tributary flow and temperatures for Bright Angel Creek, Kanab Creek and Havasu Creek (all within the East Central Grand Canyon segment) during this time. As a result, our estimates of

median flows and application of monthly average tributary temperatures used during this period resulted in overestimates of discharge at the most downstream gage (RM225) and contributed to underestimates of temperatures for those segments. Temperature predictions using a simple radiation scheme were much worse during the low flow period, exemplifying the need to have detailed radiation in rivers with significant flow variability.

4.4. Estimated heat fluxes

While some of the heat fluxes reported here (e.g., J_f, J_e, J_c) seem very large compared to values published in the literature (e.g., Meier et al., 2003; Webb & Zhang, 2004), the conditions present in the Colorado River within Grand Canyon are somewhat unique (e.g., high air temperature and cold hypolimnetic releases, large variability in discharge, and a very deep canyon that limits solar warming). Particularly, heat generated from internal fluid shear friction is often considered an insignificant source of heat in process-based river temperature models (Dugdale et al., 2017; Moore et al., 2005; Theurer et al., 1984). However, we found this flux to be important given the relatively large discharges in Grand Canyon. On average, friction made up 7% of the total heat budget, which is similar to the contributions from J_e and J_c (Table 1). Webb and Zhang (1997) found that friction provided significant heat for many streams when they conducted a heat budget analysis for 11 river segments in the Exe Basin of Devon, UK. Their work showed that average daily values of heat gained from friction accounted for 1.7 to 81.4% of the total heat energy gains to the rivers. Similarly, Meier et al. (2003) reported friction being significant in streams steeper than 5 to 10%, with a mean flux of 1812 W/m^2 in the Brenno del Lucomagno. While the average gradient of the Colorado River is 0.0015 in Grand Canyon (Wiele & Smith, 1996), the relatively high discharge compared to that of steep mountain streams (e.g., natural discharge of Brenno del Lucomagno is 2.5 m^3/s), results in similar magnitudes and relative contributions of friction reported in these studies (Table 1).

4.5. Sensitivity analysis

Perturbations in T_{BC}, averaged seasonally over the entire simulation period, have the most influence over river temperature between Lees Ferry and RM30, before the system has had sufficient exposure to weather inputs (Figure 7; Figure S10). However, at further downstream locations, changes of ± 10% in Q_{BC} resulted in a high variability in temperature residuals and often larger magnitude minimum and maximum residuals than other perturbations. Depending on the season, $J_{sn,net}$ or T_{air} can become the most influential input influencing river temperatures at RM225, as indicated by their median values. It is important to note, however, that the temperature variability caused by perturbations of these parameters is typically less than the temperature variability from ± 10% Q_{BC}. The high temperature variability from ± 10% Q_{BC} highlights the importance of correctly handling the flow balance. Similarly, the observed seasonal influence of $J_{sn,net}$, combined with the comparison between simple and detailed models (Figures 4 and S7), further illustrates the need for detailed spatiotemporal estimates of individual shortwave radiation terms when considering canyon-bound rivers.

With concerns of ecosystem management prevalent in Grand Canyon, knowing the spatial ramifications of perturbations of inputs can help interpret results and inform management decisions. Our results show that seasonal and hydrologic characteristics play a large role in determining which parameter, namely Q_{BC}, $J_{sn,net}$, or T_{air}, has the largest influence on river temperatures in downstream segments (e.g., RM225). However, perturbations of T_{BC} had the greatest effect on river temperatures near RM61, regardless of season, which is a primary habitat location of federally endangered native humpback chub

Gila cypha. This suggests that management decisions at Glen Canyon Dam could be designed to produce beneficial temperatures for native fish habitat within these upper sections of the river. The Glen Canyon Dam Adaptive Management Program (GCDAMP) have conducted experimental flow operations to investigate the creation of habitat such as sandbars and associated backwaters to promote juvenile fish growth and survival (Schmidt et al., 2007; Trammell et al., 2002). However, Dodrill et al. (2015) found that only a small proportion of the entire juvenile humpback chub population resided within backwaters. Dodrill et al. (2015) also pointed out that the observed increases in humpback chub population since 2006 (Van Haverbeke et al., 2013) occurred during a period of low backwater abundance, suggesting that population increases are likely linked to other factors such as temperature, non-native salmonid abundances, food availability, and/or turbidity. Research directly focused on growth and survival of juvenile humpback chub (Yackulic et al., 2018) and growth of sub-adult humpback chub (Dzul et al., 2016), has shown that temperature is the dominant physical factor influencing early life history demography in this river segment and success at these vulnerable life stages is essential for a healthy humpback chub population (Yackulic et al., 2014).

Within the Colorado River basin, climate change will impact the reservoir storage levels in Lake Powell as annual snowfall totals are reduced, the timing of spring snowmelt runoff shifts to earlier in the year, and overall basin runoff is decreased (Dettinger et al., 2015; Udall & Overpeck, 2017). Additionally, while efficiency trends have curtailed consumptive water use nationally since 1980 (Georgakakos et al., 2014; Maupin et al., 2014), water demands are projected to increase as population growth and climate change continue (Brown et al., 2013). With the anticipated changes to basin hydrology combined with changes in water demand, it is expected that many reservoirs will face high variability in water storage and may be relatively low for long periods of time (Barnett et al., 2004). This leaves uncertainty in the downstream thermal regime of the river as Lake Powell levels decline, resulting in warm water releases out of Glen Canyon Dam. While warm water releases are generally thought as being beneficial to native fish species that evolved under warmer thermal regimes, there are still unknown risks associated with increasing water temperatures in regard to non-native fish species. Specifically, warmer river temperatures may result in expanding the distribution and abundance of warm water non-native fishes (i.e., smallmouth bass *Micropterus dolomieu*, green sunfish *Lepomis cyanellus*, and walleye *Stizostedion vitreum*) within Grand Canyon that could swim upstream from Lake Mead, come down from Lake Powell through hydropower penstocks, or enter through accidental introductions at tributary headwaters. While the ecosystem impacts of different thermal regimes remain uncertain, understanding which mechanisms control downstream river temperature changes provides a framework for evaluating the potential ecosystem responses to changing climate and hydrology.

5. Conclusions

Canyon-bound rivers are disproportionally affected by water development, often resulting in dramatic changes to the natural downstream hydrologic and thermal characteristics, and by extension, the downstream aquatic ecosystems. As ongoing climate change exposes dammed systems to new hydrologic patterns and thermal regimes, downstream river segments may be further altered. In order to anticipate the associated changes in aquatic ecosystems, the dominant heat transfer mechanisms in canyon-bound rivers, particularly below reservoirs, need to be understood. Using process-based modeling that incorporates the influences of complex topography on radiation balances, we predicted discharge and temperature throughout the Grand Canyon over an 18-year period. The relative contribution from most of the heat fluxes (9 of the 12) represented within the model were

highly variable over time and space, indicating the dynamic nature of heating and cooling mechanisms in these systems. This is largely due to the wide range of conditions experienced over the long simulation time, the controls on net shortwave radiation (i.e., $J_{sn\text{-}net}$) due to topographic shading, and the high variability in flow releases (i.e., Q_{BC}) out of Glen Canyon Dam. In the upper portion of the model domain (RM30 and RM61), perturbations to the boundary condition water temperature (i.e., T_{BC}) had the most influence on river temperatures regardless of the time of year, while further downstream (RM88, RM167, and RM225), perturbations to the boundary condition flow (Q_{BC}), net shortwave radiation, and air temperature were dominant, but varied significantly by season. Evaluating high and low flow periods revealed that the model performed well during either condition, but highlighted the importance of having accurate tributary information during the low flow period.

Overall, the sensitivity analysis to input climate and hydrologic parameters provides a means for understanding the temporal and spatial variation in heat flux contributions in a canyon-bound river. Terrain in these environments can dramatically reduce the amount of shortwave radiation and elevate the importance of other radiative or typically less influential heat flux mechanisms. Other rivers around the world are situated similarly in deep canyons or mountainous terrain with flows highly influenced by upstream reservoir operations. These systems and their downstream segments face similar ecosystem challenges imposed by climate change as reservoir levels decline and release temperatures increase. The modeling approach presented here provides insight regarding potential climate change impacts to canyon-bound rivers and allows for thorough planning among diverse stakeholders.

Acknowledgements

Funding was provided by the Walton Family Foundation, David Bonderman, My Good Fund, and the National Science Foundation (EAR- 1343861). Any use of trade, product, or firm names is for descriptive purposes only and does not imply endorsement by the U.S. Government. Thanks to the GCMRC staff for assistance in data collection (Maria Dzul), insights and discussions on data and modeling results (Kimberly Dibble, Theodore Kennedy, Nick Voichick, and Bridget Deemer) and help with our shading model (Mike Yard and Glenn Bennett). Additional thanks to Joshua Walston at the DRI for help in acquiring shortwave radiation data. Data and models are provided online at https://www.hydroshare.org/resource/5199f53238134cc9bf4c4e997312125b/.

References

Alvarez, L. V., & Schmeeckle, M. W. (2013). Erosion of river sandbars by diurnal stage fluctuations in the Colorado River in the Marble and Grand Canyons: Full-scale laboratory experiments. River Research and Applications, 29(7), 839–854. https://doi.org/10.1002/rra.2576

Anderson, C. R., & Wright, S. A. (2007). Development and application of a water temperature model for the Colorado River below Glen Canyon Dam, Arizona. Proceedings of the American Institute of Hydrology, 23, 1–11.

Barnett, T., Malone, R., Pennell, W., Stammer, D., Semtner, B., & Washington, W. (2004). The effects of climate change on water resources in the west: Introduction and overview. Climatic Change, 62(1–3), 1–11. https://doi.org/10.1023/B:CLIM.0000013695.21726.b8

Behn, K. E., Kennedy, T. A., & Hall, R. O. J. (2010). Basal resources in backwaters of the Colorado River below Glen Canyon Dam - Effects of discharge regimes and comparison with mainstem depositional environments. U.S. Geological Survey Open-File Report 2010-1075, 25. http://pubs.usgs.gov/of/2010/1075/

Benyahya, L., Caissie, D., Satish, M. G., & El-Jabi, N. (2012). Long-wave radiation and heat flux estimates within a small tributary in Catamaran Brook (New Brunswick, Canada). Hydrological Processes, 26(4), 475–484. https://doi.org/10.1002/hyp.8141

Brazel, A. J., & Marcus, M. G. (1987). Heat enhancement by longwave wall emittance. Geographical Review, 77(4), 440. https://doi.org/10.2307/214283

Brewster, Q. M. (1992). Thermal radiative transfer and properties. John Wiley & Sons Ltd.

Brown, T. C., Foti, R., & Ramirez, J. A. (2013). Projected freshwater withdrawals in the United States under a changing climate. Water Resources Research, 49(3), 1259–1276. https://doi.org/10.1002/wrcr.20076

Buahin, C. A., & Horsburgh, J. S. (2018). Advancing the Open Modeling Interface (OpenMI) for integrated water resources modeling. Environmental Modelling & Software, 108(April), 133–153. https://doi.org/10.1016/j.envsoft.2018.07.015

Buahin, C. A., Horsburgh, J. S., & Neilson, B. T. (2019). Parallel multi-objective calibration of a component-based river temperature model. Environmental Modelling & Software, 116(February), 57–71. https://doi.org/10.1016/j.envsoft.2019.02.012

Budhu, M., & Gobin, R. (1995). Seepage-induced slope failures on sandbars in Grand Canyon. Journal of Geotechnical Engineering, 121(August), 601–609.

Buendia, C., Sabater, S., Palau, A., Batalla, R. J., & Marcé, R. (2015). Using equilibrium temperature to assess thermal disturbances in rivers. Hydrological Processes, 29(19), 4350–4360. https://doi.org/10.1002/hyp.10489

Caissie, D. (2006). The thermal regime of rivers: A review. Freshwater Biology, 51(8), 1389–1406. https://doi.org/10.1111/j.1365-2427.2006.01597.x

Caissie, D. (2016). River evaporation, condensation and heat fluxes within a first-order tributary of Catamaran Brook (New Brunswick, Canada). Hydrological Processes, 30(12), 1872–1883. https://doi.org/10.1002/hyp.10744

Cardenas, M. B., Doering, M., Rivas, D. S., Galdeano, C., Neilson, B. T., & Robinson, C. T. (2014). Analysis of the temperature dynamics of a proglacial river using time-lapse thermal imaging and energy balance modeling. Journal of Hydrology, 519(PB), 1963–1973. https://doi.org/10.1016/j.jhydrol.2014.09.079

Carpenter, M. C., Crosswhite, J. A., & Carruth, R. L. (1995). Water-level fluctuations, water temperatures, and tilts in sandbars -6.5R, 43.1L, and 172.3L, Grand Canyon, Arizona, 1990-93. Open-File Report 94-485, 17.

Carron, J. C. (2000). Simulation and optimization of unsteady flow and water temperature in reservoir regulated rivers. Civil, Environmental and Architectual Engineering Ph.D. Thesis, University of Colorado, Boulder CO., 159.

Carron, J. C., & Rajaram, H. (2001). Impact of variable reservoir releases on management of downstream water temperatures. Water Resources Research, 37(6), 1733–1743. https://doi.org/10.1029/2000WR900390

Caster, J. J., Dealy, T. P., Andrews, T., Fairley, H., Draut, A. E., Sankey, J. B., & Bedford, D. R. (2014). Meteorological data for selected sites along the Colorado River Corridor, Arizona, 2011-2013. U.S. Geological Survey Open-File Report 2014-1247, 56. https://doi.org/http://dx.doi.org/10.3133/ofr20141247

Caster, J. J., & Sankey, J. B. (2016). Variability in rainfall at monitoring stations and derivation of a long-term rainfall intensity record in the Grand Canyon Region, Arizona, USA. In Scientific Investigations Report. https://doi.org/10.3133/sir20165012

Chapra, S. C. (1997). Surface water-quality modeling. In McGraw-Hill Series in Water Resources and Environmental Engineering.

Chen, Y. D., Carsel, R. F., McCutcheon, S. C., & Nutter, W. L. (1998a). Stream temperature simulation of forested riparian areas: I. Watershed-scale model development. Journal of Environmental Engineering, 124(4), 304–315. https://doi.org/10.1061/(ASCE)0733-9372(1998)124:4(304)

Chen, Y. D., McCutcheon, S. C., Norton, D. J., & Nutter, W. L. (1998b). Stream temperature simulation of forested riparian areas: II. Model application. Journal of Environmental Engineering, 124(4), 316–328. https://doi.org/10.1061/(ASCE)0733-9372(1998)124:4(316)

Chen, Y., Hall, A., & Liou, K. N. (2006). Application of three-dimensional solar radiative transfer to mountains. Journal of Geophysical Research, 111(D21), D21111. https://doi.org/10.1029/2006JD007163

Collier, M., Webb, R. H., & Schmidt, J. C. (1996). Dams and rivers: a primer on the downstream effects of dams. US Geological Survey Circular, 1126. https://doi.org/10.3133/cir1126

Cox, M. M., & Bolte, J. P. (2007). A spatially explicit network-based model for estimating stream temperature distribution. Environmental Modelling and Software, 22(4), 502–514. https://doi.org/10.1016/j.envsoft.2006.02.011

Dervishi, S., & Mahdavi, A. (2012). Computing diffuse fraction of global horizontal solar radiation: A model comparison. Solar Energy, 86(6), 1796–1802. https://doi.org/10.1016/j.solener.2012.03.008

Dettinger, M., Udall, B., & Georgakakos, A. (2015). Western water and climate change. Ecological Applications, 25(8), 2069–2093. https://doi.org/10.1890/15-0938.1

Dodrill, M. J., Yackulic, C. B., Gerig, B., Pine, W. E., Korman, J., & Finch, C. (2015). Do management actions to restore rare habitat benefit native fish conservation? distribution of juvenile native fish among shoreline habitats of the Colorado River. River Research and Applications, 31(10), 1203–1217. https://doi.org/10.1002/rra.2842

Dozier, J., & Frew, J. (1990). Rapid calculation of terrain parameters for radiation modeling from digital elevation data. IEEE Transactions on Geoscience and Remote Sensing, 28(5), 963–969. https://doi.org/10.1109/36.58986

Draut, A. E., & Rubin, D. M. (2006). Measurements of wind, aeolian sand transport, and precipitation in the Colorado River corridor, Grand Canyon, Arizona; January 2005 to January 2006. In Open-File Report (Revised an). https://doi.org/10.3133/ofr20061188

Dubayah, R., & Rich, P. M. (1995). Topographic solar radiation models for GIS. International Journal of Geographical Information Systems, 9(4), 405–419. https://doi.org/10.1080/02693799508902046

Dugdale, S. J., Hannah, D. M., & Malcolm, I. A. (2017). River temperature modelling: A review of process-based approaches and future directions. Earth-Science Reviews, 175(October), 97–113. https://doi.org/10.1016/j.earscirev.2017.10.009

Dzul, M. C., C. B. Yackulic, J. Korman, M. D. Yard, & J. D. Muehlbauer. (2016). Incorporating temporal heterogeneity in environmental conditions into a somatic growth model. Canadian Journal of Fisheries and Aquatic Sciences:1-11

Edinger, J. E., Duttweiler, D. W., & Geyer, J. C. (1968). The response of water temperatures to meteorological conditions. Water Resources Research. https://doi.org/10.1029/WR004i005p01137

Erbs, D. G., Klein, S. A., & Duffie, J. A. (1982). Estimation of the diffuse radiation fraction for hourly, daily and monthly-average global radiation. Solar Energy. https://doi.org/10.1016/0038-092X(82)90302-4

Ferencz, S. B., Cardenas, M. B., & Neilson, B. T. (2019). Analysis of the effects of dam release properties and ambient groundwater flow on surface water-groundwater exchange over a 100-km-long reach. Water Resources Research, 55(11), 8526–8546. https://doi.org/10.1029/2019WR025210

Ferrari, R. (1987). Colorado River water temperature modeling below Glen Canyon Dam. *Glen Canyon Environmental Studies*.

Fitzgerald, J. (1996). Residence time of groundwater issuing from the South Rim Aquifer in the eastern Grand Canyon. Department of Geoscience MSc Thesis, University of Nevada, Las Vegas.

Garrett, D., Baron, J., Dale, V., Gunderson, L., Hulse, D., Kitchell, J., Loomis, J., Palmer, M., Parker, R., Robertson, D., Schwartz, D., & Watkins, J. (2003). Evaluating a Glen Canyon Dam temperature control device to enhance native fish habitat in the Colorado River: A risk assessment. Upper Colorado Region, Bureau of Reclamation, June.

Gates, D. M. (1980). Biophysical ecology. Springer New York, 611p. https://doi.org/10.1007/978-1-4612-6024-0

Georgakakos, A., Fleming, P., Dettinger, M., Peters-Lidard, C., Richmond, T. (T. C. ., Reckhow, K., White, K., & Yates, D. (2014). Ch. 3: Water resources. Climate change impacts in the United States: The third national climate assessment. https://doi.org/10.7930/J0G44N6T

Gloss, S., Lovich, J., & Melis, T. (2005). The State of the Colorado River Ecosystem in Grand Canyon: USGS Circular 1282.

Goings, D. B. (1985). Spring flow in a portion of Grand Canyon National Park, Arizona. Department of Geoscience MSc Thesis, University of Nevada, Las Vegas.

Graf, J. B. (1995). Measured and Predicted Velocity and Longitudinal Dispersion At Steady and Unsteady-Flow, Colorado River, Glen Canyon Dam To Lake Mead. Water Resources Bulletin, 31(2), 265–281.

Graff, W. (1999). Dam Nation: A Geographic Census of American Dams and Their Large-Scale Hydrologic Impacts. 35(4), 1305–1311.

Grams, P., Schmidt, J., Wright, S., Topping, D., Melis, T., & Rubin, D. (2015). Building sandbars in the Grand Canyon. Eos, 96. https://doi.org/10.1029/2015EO030349

Gu, R., Montgomery, S., & Austin, T. AL. (1998). Quantifying the effects of stream discharge on summer river temperature. Hydrological Sciences Journal, 43(6), 885–904. https://doi.org/10.1080/02626669809492185

Hoch, S. W., & David Whiteman, C. (2010). Topographic effects on the surface radiation balance in and around Arizona's Meteor crater. Journal of Applied Meteorology and Climatology, 49(6), 1114–1128. https://doi.org/10.1175/2010JAMC2353.1

Hoffnagle, T. L. (2001). Changes in water temperature of backwaters during fluctuating vs. short-term steady flows in the Colorado River, Grand Canyon. Proceedings of the Fifth Biennial Conference of Research on the Colorado Plateau, June, 103–118.

Huning, L. S., & Margulis, S. A. (2015). Watershed modeling applications with a modular physically-based and spatially-distributed watershed educational toolbox. Environmental Modelling & Software, 68, 55–69. https://doi.org/10.1016/j.envsoft.2015.02.008

Huntoon, P. W. (1974). The karstic groundwater basins of the Kaibab Plateau, Arizona. Water Resources Research, 10(3), 579–590. https://doi.org/10.1029/WR010i003p00579

Karlstrom, K. E., Timmons, J. M., & Crossey, L. J. (2012). Introduction to Grand Canyon geology. Special Paper of the Geological Society of America, 489(November), 1–6. https://doi.org/10.1130/2012.2489(00)

King, T. V., & Neilson, B. T. (2019). Quantifying reach-average effects of hyporheic exchange on arctic river temperatures in an area of continuous permafrost. Water Resources Research, 1–21. https://doi.org/10.1029/2018WR023463

Kurylyk, B. L., Moore, R. D., & Macquarrie, K. T. B. (2016). Scientific briefing: Quantifying streambed heat advection associated with groundwater-surface water interactions. Hydrological Processes. https://doi.org/10.1002/hyp.10709

Lam, J. C., & Li, D. H. W. (1996). Correlation between global solar radiation and its direct and diffuse components. Building and Environment, 31(6), 527–535. https://doi.org/10.1016/0360-1323(96)00026-1

Larson, D. W., Matthes, U., & Kelly, P. E. (2000). Cliff ecology: pattern and process in cliff ecosystems. Cambridge, 360p. https://doi.org/10.5860/CHOICE.37-6277

Leach, J. A., & Moore, R. D. (2010). Above-stream microclimate and stream surface energy exchanges in a wildfire-disturbed riparian zone. Hydrological Processes, 24(17), 2369–2381. https://doi.org/10.1002/hyp.7639

Leeder, M. R. (2010). Sedimentology and sedimentary basins: From turbulence to tectonics. *Wiley*.

Loinaz, M. C., Davidsen, H. K., Butts, M., & Bauer-Gottwein, P. (2013). Integrated flow and temperature modeling at the catchment scale. Journal of Hydrology, 495, 238–251. https://doi.org/10.1016/j.jhydrol.2013.04.039

Lowney, C. L. (2000). Stream temperature variation in regulated rivers: Evidence for a spatial pattern in daily minimum and maximum magnitudes. Water Resources Research, 36(10), 2947–2955. https://doi.org/10.1029/2000WR900142

MacDonald, R. J., Boon, S., & Byrne, J. M. (2014). A process-based stream temperature modelling approach for mountain regions. Journal of Hydrology, 511, 920–931. https://doi.org/10.1016/j.jhydrol.2014.02.009

Magirl, C. S., Breedlove, Mi. J., Webb, R. H., & Griffitsh, P. G. (2008). Modeling water-surface elevations and virtual shorelines for the Colorado River in Grand Canyon, Arizona. U.S. Geological Survey, Scientific Investigations Report, 2008–5075, 1–32.

Magirl, C. S., Webb, R. H., & Griffiths, P. G. (2005). Changes in the water surface profile of the Colorado River in Grand Canyon, Arizona, between 1923 and 2000. Water Resources Research, 41(5), 1–10. https://doi.org/10.1029/2003WR002519

Matzinger, N., Andretta, M., van Gorsel, E., Vogt, R., Ohmura, A., & Rotach, M. W. (2003). Surface radiation budget in an alpine valley. Quarterly Journal of the Royal Meteorological Society, 129(588), 877–895. https://doi.org/10.1256/qj.02.44

Maupin, M. A., Kenny, J. F., Hutson, S. S., Lovelace, J. K., Barber, N. L., & Linsey, K. S. (2014). Estimated use of water in the United States in 2010. https://doi.org/http://dx.doi.org/10.3133/cir1405

McMahon, A., & Moore, R. D. (2017). Influence of turbidity and aeration on the albedo of mountain streams. Hydrological Processes, 31(25), 4477–4491. https://doi.org/10.1002/hyp.11370

Meier, W., Bonjour, C., Wüest, A., & Reichert, P. (2003). Modeling the effect of water diversion on the temperature of mountain streams. Journal of Environmental Engineering, 129(8), 755–764. https://doi.org/10.1061/(ASCE)0733-9372(2003)129:8(755)

Melis, T. S. (Editor) (2011). Effects of three high-flow experiments on the Colorado River ecosystem downstream from Glen Canyon Dam, Arizona. U.S. Geological Survey Circular, 1366 (February), 147 p. http://pubs.usgs.gov/circ/1366/

Moore, R. D., Leach, J. A., & Knudson, J. M. (2014). Geometric calculation of view factors for stream surface radiation modelling in the presence of riparian forest. Hydrological Processes, 28(6), 2975–2986. https://doi.org/10.1002/hyp.9848

Moore, R. D., Spittlehouse, D. L., & Story, A. (2005). Riparian microclimate and stream temperature response to forest harvesting: A review. Journal of the American Water Resources Association, 41(4), 813–834. https://doi.org/10.1111/j.1752-1688.2005.tb03772.x

Neilson, B. T., Stevens, D. K., Chapra, S. C., & Bandaragoda, C. (2009). Data collection methodology for dynamic temperature model testing and corroboration. Hydrological Processes, 23(20), 2902–2914. https://doi.org/10.1002/hyp.7381

Neilson, B. T., Stevens, D. K., Chapra, S. C., & Bandaragoda, C. (2010). Two-zone transient storage modeling using temperature and solute data with multiobjective calibration: 1. Temperature. Water Resources Research, 46(12), 1–17. https://doi.org/10.1029/2009WR008759

Nilsson, C., & Renöfält, B. M. (2008). Linking Flow Regime and Water Quality in Rivers: a Challenge to Adaptive Catchment Management. Ecology and Society, 13(2), art18. https://doi.org/10.5751/ES-02588-130218

Olden, J. D., & Naiman, R. J. (2010). Incorporating thermal regimes into environmental flows assessments: Modifying dam operations to restore freshwater ecosystem integrity. Freshwater Biology, 55(1), 86–107. https://doi.org/10.1111/j.1365-2427.2009.02179.x

Olyphant, G. A. (1986). Longwave radiation in mountainous areas and its influence on the energy balance of alpine snowfields. Water Resources Research, 22(1), 62–66. https://doi.org/10.1029/WR022i001p00062

Orgill, J. F., & Hollands, K. G. T. (1977). Correlation equation for hourly diffuse radiation on a horizontal surface. Solar Energy, 19(4), 357–359. https://doi.org/10.1016/0038-092X(77)90006-8

Petersen, J. H., & Paukert, C. P. (2005). Development of a bioenergetics model for humpback chub and evaluation of water temperature changes in the Grand Canyon, Colorado River. Transactions of the American Fisheries Society, 134(4), 960–974. https://doi.org/10.1577/T04-090.1

Plüss, C., & Ohmura, A. (1997). Longwave radiation on snow-covered mountainous surfaces. Journal of Applied Meteorology, 36(6), 818–824. https://doi.org/10.1175/1520-0450-36.6.818

Polehn, R. A., & Kinsel, W. C. (1997). Transient temperature solution for stream flow from a controlled temperature source. Water Resources Research, 33(1), 261–265. https://doi.org/10.1029/96WR03016

Risley, J. C., Constantz, J., Essaid, H., & Rounds, S. (2010). Effects of upstream dams versus groundwater pumping on stream temperature under varying climate conditions. Water Resources Research, 46(6). https://doi.org/10.1029/2009WR008587

Ross, R. P., & Vernieu, W. S. (2013). Nearshore temperature findings for the Colorado River in Grand Canyon, Arizona - Possible implications for native fish. U.S. Geological Survey Fact Sheet 2013–3104. https://doi.org/10.3133/fs20133104

Rossman, L. A. (2006). Storm water management model quality assurance report: Dynamic wave flow routing. Storm Water Management Model Quality Assurance Report, EPA/600/R-06/097, 1–115. http://www.epa.gov/water-research/storm-water-management-model-swmm

Roth, T. R., Westhoff, M. C., Huwald, H., Huff, J. A., Rubin, J. F., Barrenetxea, G., Vetterli, M., Parriaux, A., Selker, J. S., & Parlange, M. B. (2010). Stream temperature response to three riparian vegetation scenarios by use of a distributed temperature validated model. Environmental Science & Technology, 44(6), 2072–2078. https://doi.org/10.1021/es902654f

Rutherford, J. C., Blackett, S., Blackett, C., Saito, L., & Davies-Colley, R. J. (1997). Predicting the effects of shade on water temperature in small streams. New Zealand Journal of Marine and Freshwater Research, 31(5), 707–721. https://doi.org/10.1080/00288330.1997.9516801

Sabol, T. A., & Springer, A. E. (2013). Transient simulation of groundwater levels within a sandbar of the Colorado River, Marble Canyon, Arizona, 2004. U.S. Geological Survey Open-File Report 2013-1277, 22. https://doi.org/http://dx.doi.org/10.3133/ofr20131277

Schmidt, J. C., Topping, D. J., Rubin, D. M., Hazel, J. E., Kaplinski, M., Wiele, S. M., & Goeking, S. A. (2007). Streamflow and sediment data collected to determine the effects of low summer steady flows and habitual maintenance flows in 2000 on the Colorado River between Lees Ferry and Bright Angel Creek, Arizona. U.S. Geological Survey Open-File Report 2007-1268, 79 p. http://pubs.usgs.gov/of/2007/1268/

Sridhar, V., Sansone, A. L., LaMarche, J., Dubin, T., & Lettenmaier, D. P. (2004). Prediction of stream temperature in forested watersheds. Journal of the American Water Resources Association, 40(1), 197–213. https://doi.org/10.1111/j.1752-1688.2004.tb01019.x

Stanitski-Martin, D. (1996). Seasonal energy balance relationships over the Colorado River and adjacent riparian habitat: Glen Canyon, Arizona. Ph.D. Dissertation, Arizona State University, Tempe. https://doi.org/10.16953/deusbed.74839

Theurer, F. D., Voos, K. A., & Miller, W. J. (1984). Instream water temperature model. Instream Flow Information Paper 16. In FWS/OBS. http://pubs.er.usgs.gov/publication/fwsobs84_15

Topping, D. J., Rubin, D. M., & Vierra, L. E. (2000). Colorado River sediment transport: 1. Natural sediment supply limitation and the influence of Glen Canyon Dam. Water Resources Research, 36(2), 515–542. https://doi.org/10.1029/1999WR900285

Topping, D. J., Schmidt, J. C., & Vierra Jr., L. E. (2003). Computation and analysis of the instantaneous-discharge record for the Colorado River at Lees Ferry, Arizona : May 8, 1921, through September 30, 2000. In Professional Paper. https://doi.org/10.3133/pp1677

Trammell, M. A., Valdez, R. A., Carothers, S. W., & Ryel, R. J. (2002). Effects of a low steady summer flow experiment on native fishes of the Colorado River in Grand Canyon, Arizona. SWCA Environmental Consultants.

U.S. Bureau of Reclamation. (1999). Glen Canyon Dam modifications to control downstream temperatures - plan and draft environmental assessment. Department of the Interior.

U.S. Bureau of Reclamation. (2012). Colorado River Basin Water Supply and Demand Study. 85.

Udall, B., & Overpeck, J. (2017). The twenty-first century Colorado River hot drought and implications for the future. Water Resources Research, 53(3), 2404–2418. https://doi.org/10.1002/2016WR019638

U.S. Department of the Interior. (2007). Recod of decision: Colorado River interim guidelines for lower basin shortages and the coordinated operations for Lake Powell and Lake Mead, Final environmental impact statement. Office of the Secretary of Interior, Washington, D.C.

Valdez, R. A., Speas, D. W., & Kubly, D. M. (2013). Benefits and risks of temperature modification at Glen Canyon Dam to aquatic resources of the Colorado River in the Grand Canyon. U.S. Bureau of Reclamation, Upper Colorado Region, Salt Lake City, UT.

Van Haverbeke, D. R., Stone, D. M., Coggins, L. G., & Pillow, M. J. (2013). Long-term monitoring of an endangered desert fish and factors influencing population dynamics. Journal of Fish and Wildlife Management, 4(1), 163–177. https://doi.org/10.3996/082012-JFWM-071

Vernieu, W. S., & Anderson, C. R. (2013). Water temperatures in select nearshore environments of the Colorado River in Grand Canyon, Arizona, during the low steady summer flow experiment of 2000. U.S. Geological Survey Open- File Report 2013–1066, 44.

Vernieu, W. S., Hueftle, S. J., & Gloss, S. P. (2005). Water quality in Lake Powell and the Colorado River. In S. P. Gloss, J. E. Lovich, & T. S. Melis (Eds.), State of the Colorado River Ecosystem (pp. 69–85). U.S. Geological Survey Circular 1282.

Ward, J. V., & Stanford, J. A. (1983). The serial discontinuity concept of lotic ecosystems.

Wawrzyniak, V., Allemand, P., Bailly, S., Lejot, J., & Piégay, H. (2017). Coupling LiDAR and thermal imagery to model the effects of riparian vegetation shade and groundwater inputs on summer river temperature. Science of the Total Environment, 592, 616–626. https://doi.org/10.1016/j.scitotenv.2017.03.019

Webb, B. W., Hannah, D. M., Moore, R. D., Brown, L. E., & Nobilis, F. (2008). Recent advances in stream and river temperature research. Hydrological Processes, 22(7), 902–918. https://doi.org/10.1002/hyp.6994

Webb, B. W., & Walling, D. E. (1993). Temporal variability in the impact of river regulation on thermal regime and some biological implications. Freshwater Biology, 29(1), 167–182. https://doi.org/10.1111/j.1365-2427.1993.tb00752.x

Webb, B. W., & Zhang, Y. (1997). Spatial and seasonal variability in the components of the river heat budget. Hydrological Processes, 11(1), 79–101. https://doi.org/10.1002/(SICI)1099-1085(199701)11:1<79::AID-HYP404>3.0.CO;2-N

Webb, B. W., & Zhang, Y. (2004). Intra-annual variability in the non-advective heat energy budget of Devon streams and rivers. Hydrological Processes, 18(11), 2117–2146. https://doi.org/10.1002/hyp.1463

Wenzel, L. K., & Fishel, V. C. (1942). Methods for determining permeability of water-bearing materials, with special reference to discharging-well methods, with a section on direct laboratory methods and bibliography on permeability and laminar flow. USGS Water Supply Paper 887. https://doi.org/10.3133/wsp887

Westhoff, M. C., Savenije, H. H. G., Luxemburg, W. M. J., Stelling, G. S., van de Giesen, N. C., Selker, J. S., Pfister, L., & Uhlenbrook, S. (2007). A distributed stream temperature model using high resolution temperature observations. Hydrology and Earth System Sciences Discussions, 4(1), 125–149. https://doi.org/10.5194/hessd-4-125-2007

Whiteman, C. D., Allwine, K. J., Fritschen, L. J., Orgill, M. M., & Simpson, J. R. (1989). Deep valley radiation and surface energy budget microclimates. Part I: Radiation. Journal of Applied Meteorology, 28(6), 414–426. https://doi.org/10.1175/1520-0450(1989)028<0414:DVRASE>2.0.CO;2

Wiele, S. M., & Griffin, E. R. (1997). Modification to a one-dimensional model of unsteady flow in the Colorado River through the Grand Canyon, Arizona. Water-Resouces Investigations Report 97-4046, 17.

Wiele, S. M., & Smith, J. D. (1996). A reach-averaged model of diurnal discharge wave propagation down the Colorado River through the Grand Canyon. Water Resources Research, 32(5), 1375–1386. https://doi.org/10.1029/96WR00199

Wright, S. A., Anderson, C. R., & Voichick, N. (2009). A simplified water temperature model for the Colorado River below Glen Canyon Dam. River Research and Applications, 25(6), 675–686. https://doi.org/10.1002/rra.1179

Wright, S. A., Melis, T. S., Topping, D. J., & Rubin, D. M. (2005). Influence of Glen Canyon Dam operations on downstream sand resources of the Colorado River in Grand Canyon. In S. P. Gloss, J. E. Lovich, & T. S. Melis (Eds.), State of the Colorado River Ecosystem (pp. 17–31). U.S. Geological Survey Circular 1282.

Yackulic, C. B., M. D. Yard, J. Korman, & D. R. Van Haverbeke. (2014). A quantitative life history of endangered humpback chub that spawn in the Little Colorado River: variation in movement, growth, and survival. Ecology and Evolution 4:1006-1018.

Yackulic, C. B., J. Korman, M. D. Yard, & M. Dzul. (2018). Inferring species interactions through joint mark–recapture analysis. Ecology 99:812-821.

Yard, M. D., Bennett, G. E., Mietz, S. N., Coggins, L. G., Stevens, L. E., Hueftle, S., & Blinn, D. W. (2005). Influence of topographic complexity on solar insolation estimates for the Colorado River, Grand Canyon, AZ. Ecological Modelling, 183(2–3), 157–172. https://doi.org/10.1016/j.ecolmodel.2004.07.027

Zhang, Y. L., Li, X., Cheng, G. D., Jin, H. J., Yang, D. W., Flerchinger, G. N., Chang, X. L., Wang, X., & Liang, J. (2018). Influences of topographic shadows on the thermal and hydrological processes in a cold region mountainous watershed in northwest China. Journal of Advances in Modeling Earth Systems, 10(7), 1439–1457. https://doi.org/10.1029/2017MS001264

Zukosky, K. A. (1995). An assessment of the potential to use water chemistry parameters to define ground water flow pathways at Grand Canyon National Park , Arizona. Department of Geoscience MSc Thesis, University of Nevada, Las Vegas.

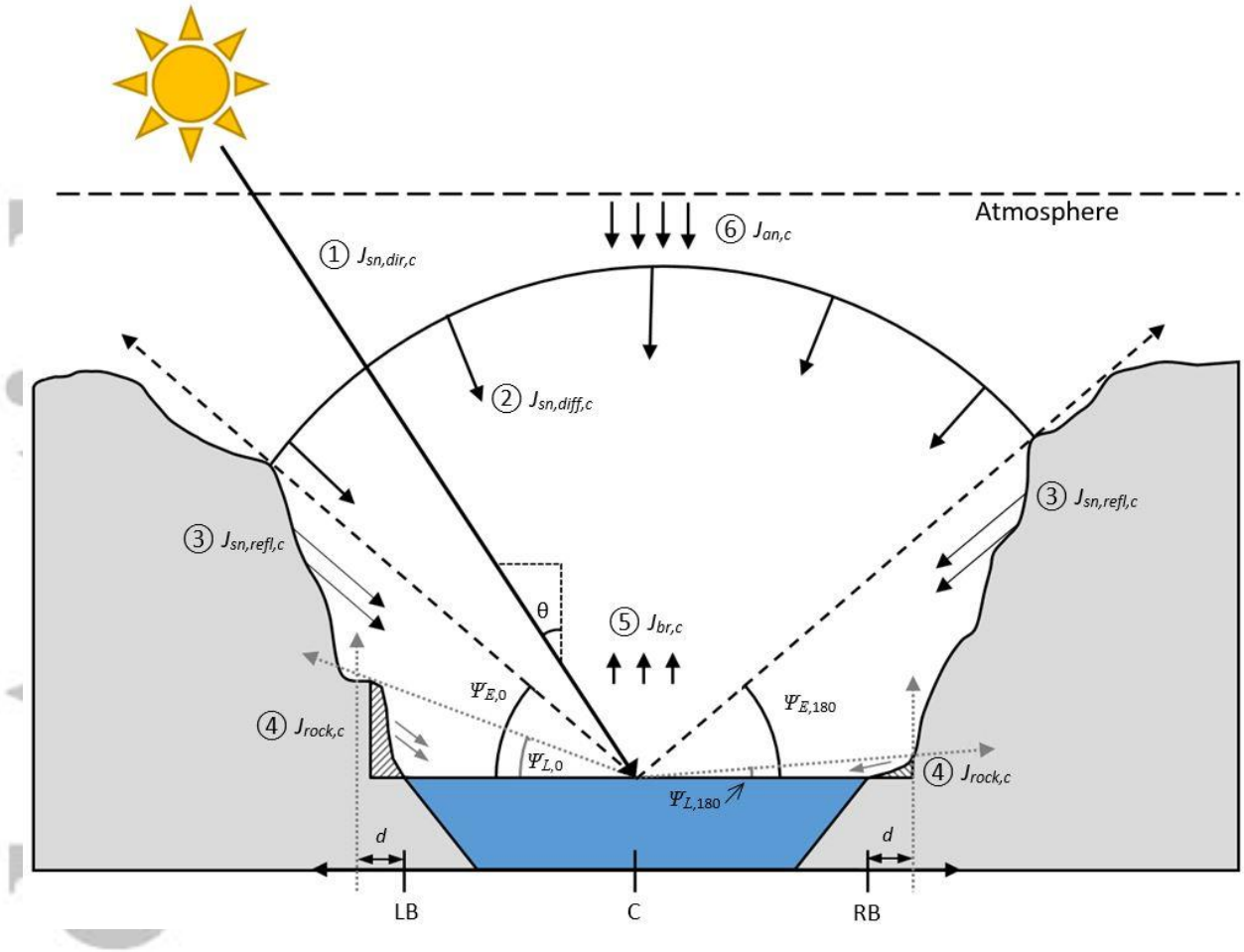

Figure 1. Schematic illustrating the radiation balance used in this model for a cross-section of the river at a given model cell (*c*). LB = left bank, RB = right bank, C = river center, d = distance in meters away from the river bank, θ = the solar zenith angle, $\Psi_{E,0}$ = is the elevation angle from river center at 0° azimuth (Φ), $\Psi_{E,180}$ = is the elevation angle from river center at Φ=180°, $\Psi_{L,0}$ = is the land re-emittance angle from river center at Φ = 0°, $\Psi_{L,180}$ = is the land re-emittance angle from river center at Φ =180°. For the radiation balance Φ is calculated from 0° to 359°, but only 0° and 180° are shown here for illustration. Shortwave radiation received at the water surface within the canyon consists of 1) direct shortwave radiation ($J_{sn,dir,c}$) originating from the sun and scaled by topographic shading factors (S_f), 2) diffuse shortwave radiation ($J_{sn,diff,c}$) originating from any sky direction as the result of scattering by atmospheric gases and particles and scaled by the sky view factor (SV_f), and 3) land-reflected longwave radiation ($J_{sn,refl,c}$) from nearby terrain. Longwave radiation components considered in this model include 4) rock longwave radiation ($J_{rock,c}$) within a specified distance (d) of the edge of water 5) water longwave radiation ($J_{br,c}$), and 6) atmospheric longwave radiation ($J_{an,c}$) scaled by the sky view factor ($SV_{f,c,d}$) calculated from the river center and including the area at a specified distance (d) from the edge of water.

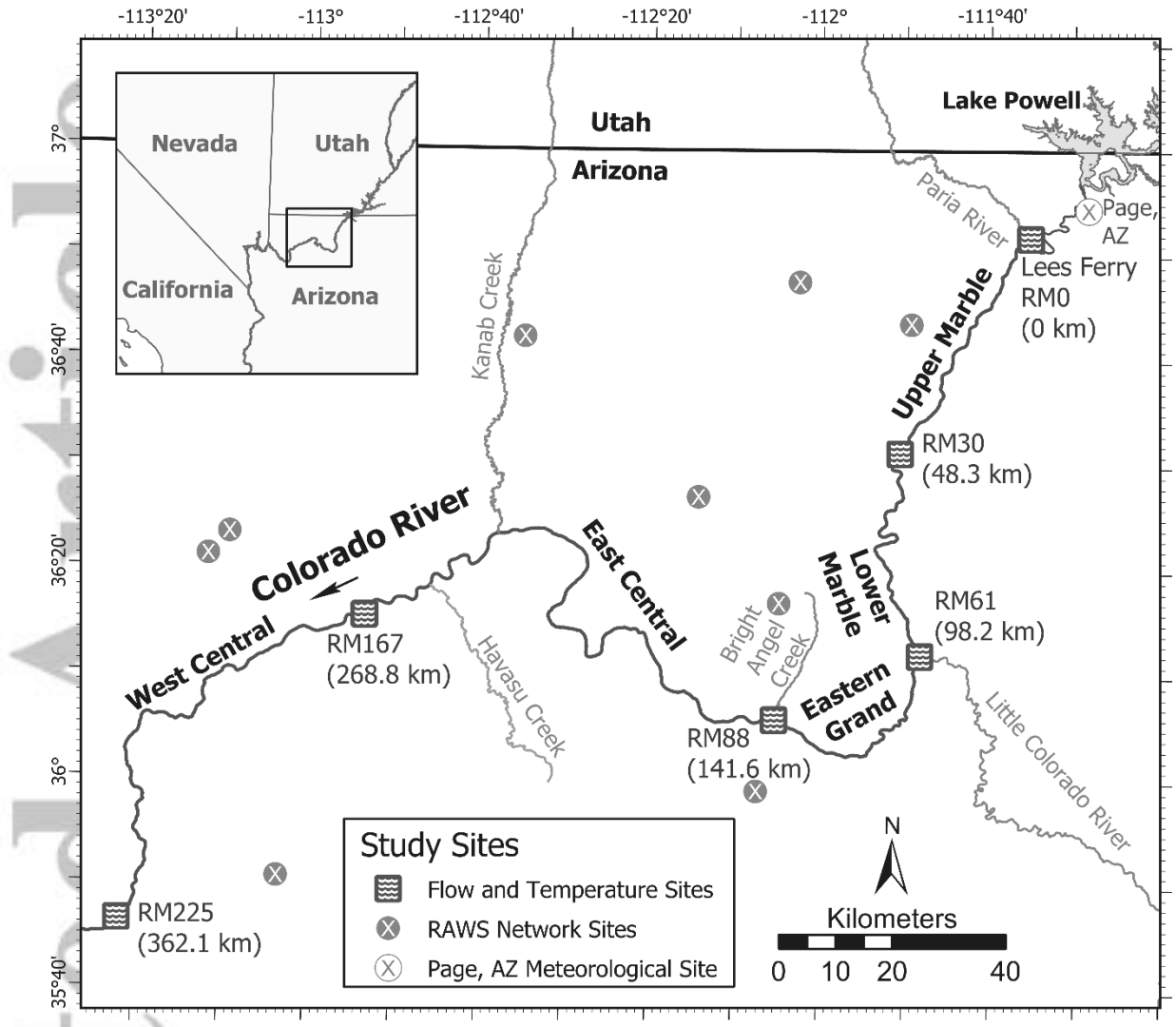

Figure 2. Map of the study area depicting model extent (RM0-RM225), major river segments (Melis, 2011), and the location of discharge and temperature monitoring sites used in the river temperature model. Only tributaries with measured discharge and temperature are shown. Note that not all remote automated weather station (RAWS) network sites used in our model are shown on this map.

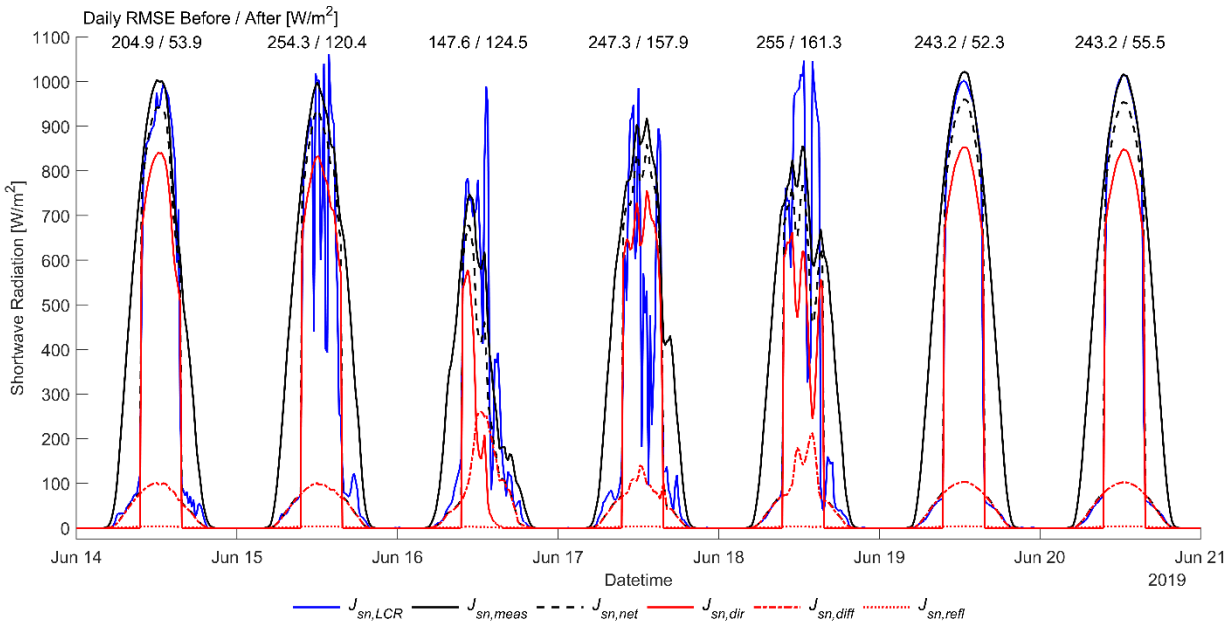

Figure 3. Comparison of shortwave radiation measurements from the LCR ($J_{sn,LCR}$) to estimated components of shortwave radiation (i.e., $J_{sn,net}$, $J_{sn,dir}$, $J_{sn,diff}$, $J_{sn,refl}$) derived from the median value of measured shortwave radiation at RAWS network sites ($J_{sn,meas}$) near the study area. Daily RMSE values are provided above each day to illustrate the influence of the diffuse radiation correlation model and correspond to the fit of $J_{sn,meas}$ to $J_{sn,LCR}$ before and after radiation scaling.

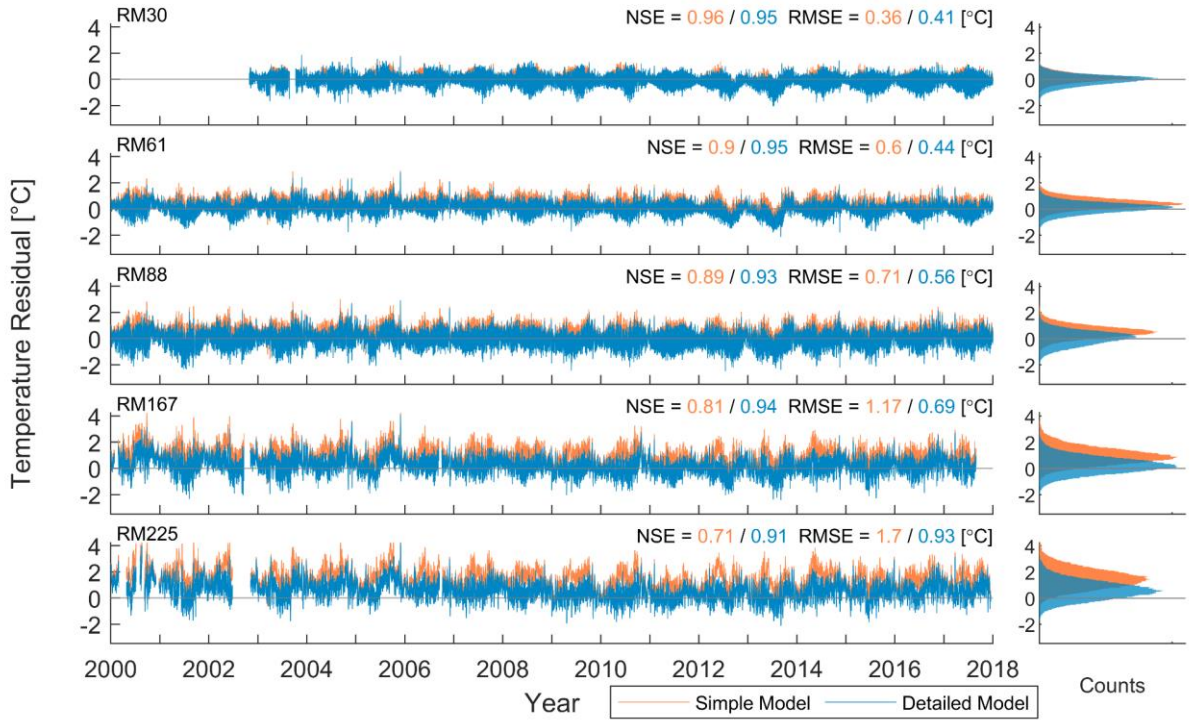

Figure 4. Plot of long-term river temperature model residuals (observed minus modeled) for the simple and detailed radiation schemes at 5 gaging stations within Grand Canyon (RM30, RM61, RM88, RM167, and RM225). The right panels show the distribution of residuals between observed and modeled temperatures in °C.

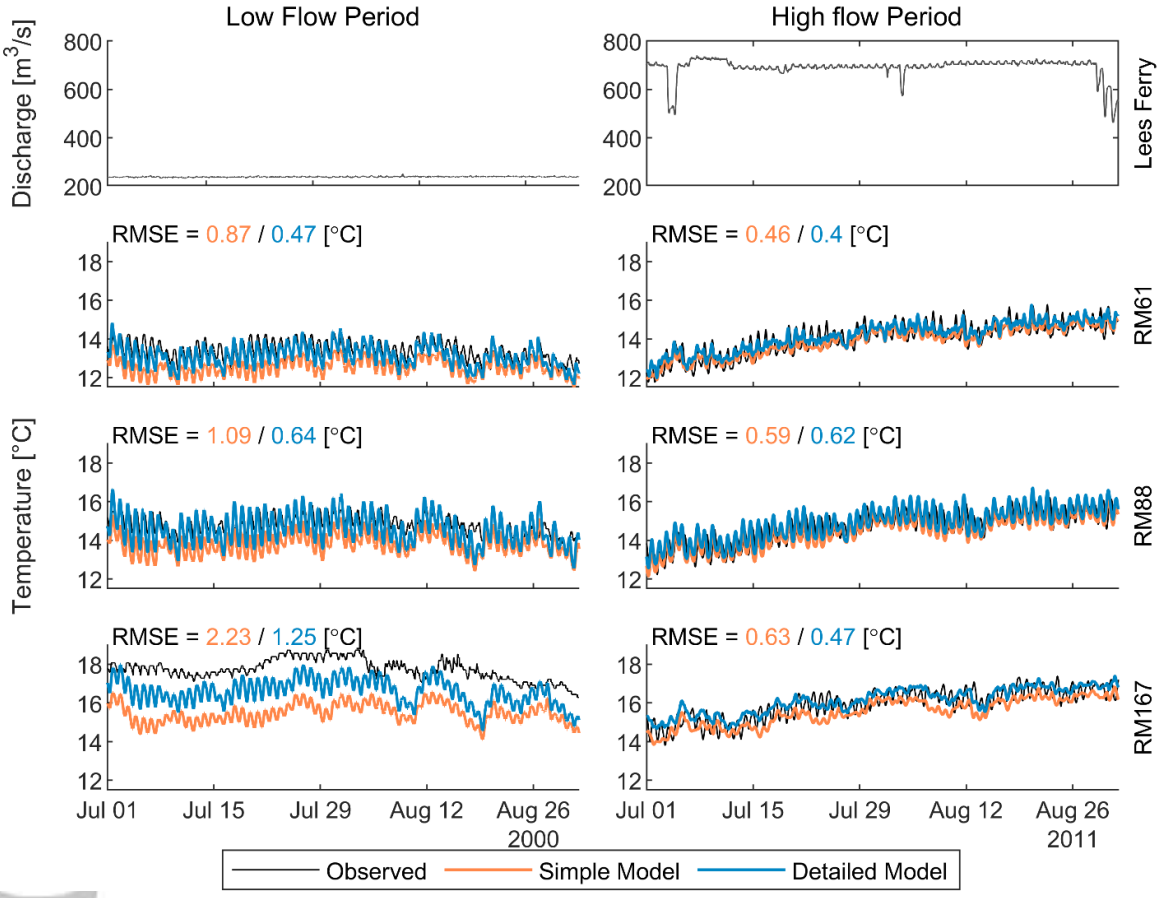

Figure 5. Comparison of model results during low flow and high flow summer periods. The left and right columns show model results for July and August of 2000 and 2011, respectively. The top row shows observed discharge at Lees Ferry. Subsequent rows from top to bottom show modeled temperature predictions and observed data at RM61, RM88, and RM167.

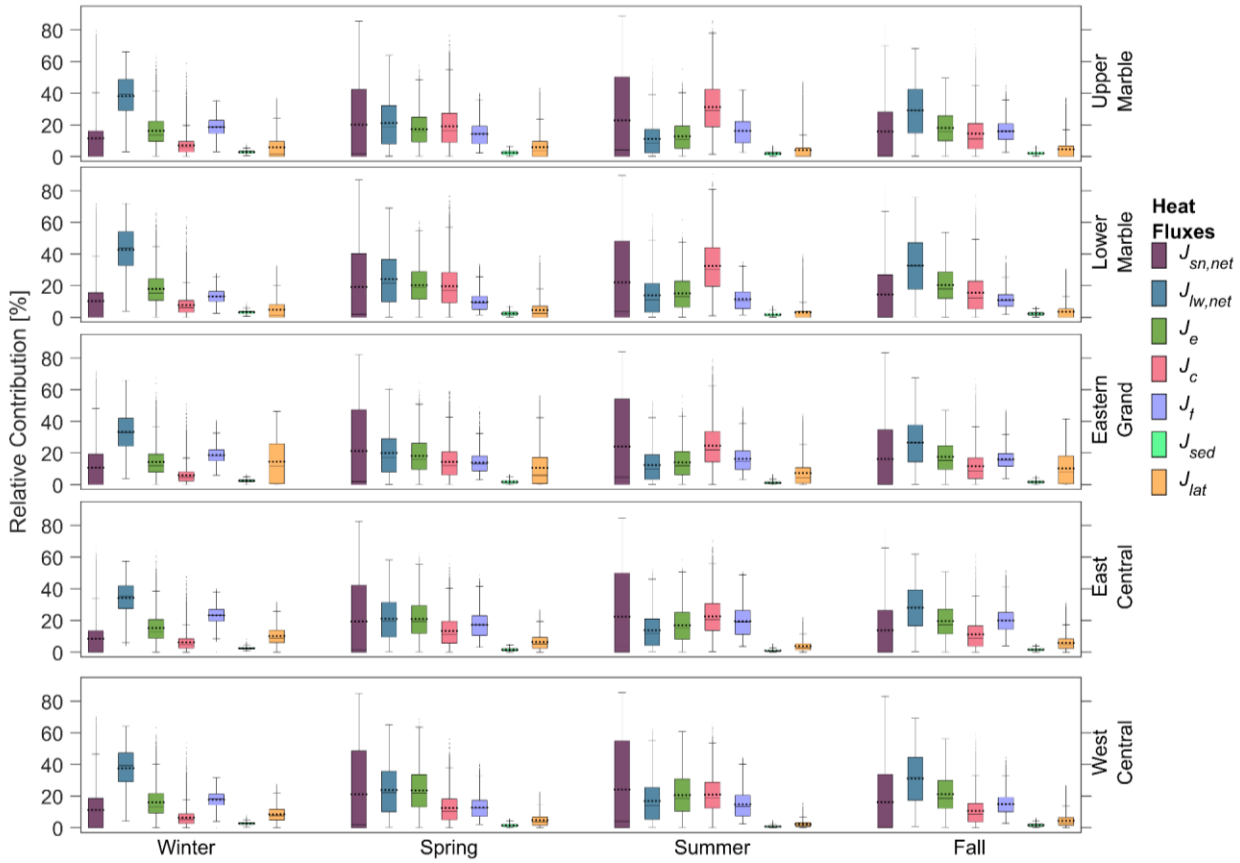

Figure 6. Boxplot of relative contribution of heat fluxes averaged over each model segment (shown in Figure 1) and each season of the year (Winter = Dec.-Feb., Spring = Mar.-May, Summer = Jun.-Aug., and Fall = Sep.-Nov.) for the entire simulation period. Mean values are included as horizontal dots. Shortwave and longwave radiative heat fluxes and lateral sources have been combined for readability. Variables being compared are net shortwave radiation ($J_{sn,net}$), net longwave radiation ($J_{lw,net}$), latent heat (J_e), sensible heat (J_c), friction (J_f), bed conduction (J_{sed}), and the apparent sensible heat from lateral sources (J_{lat}).

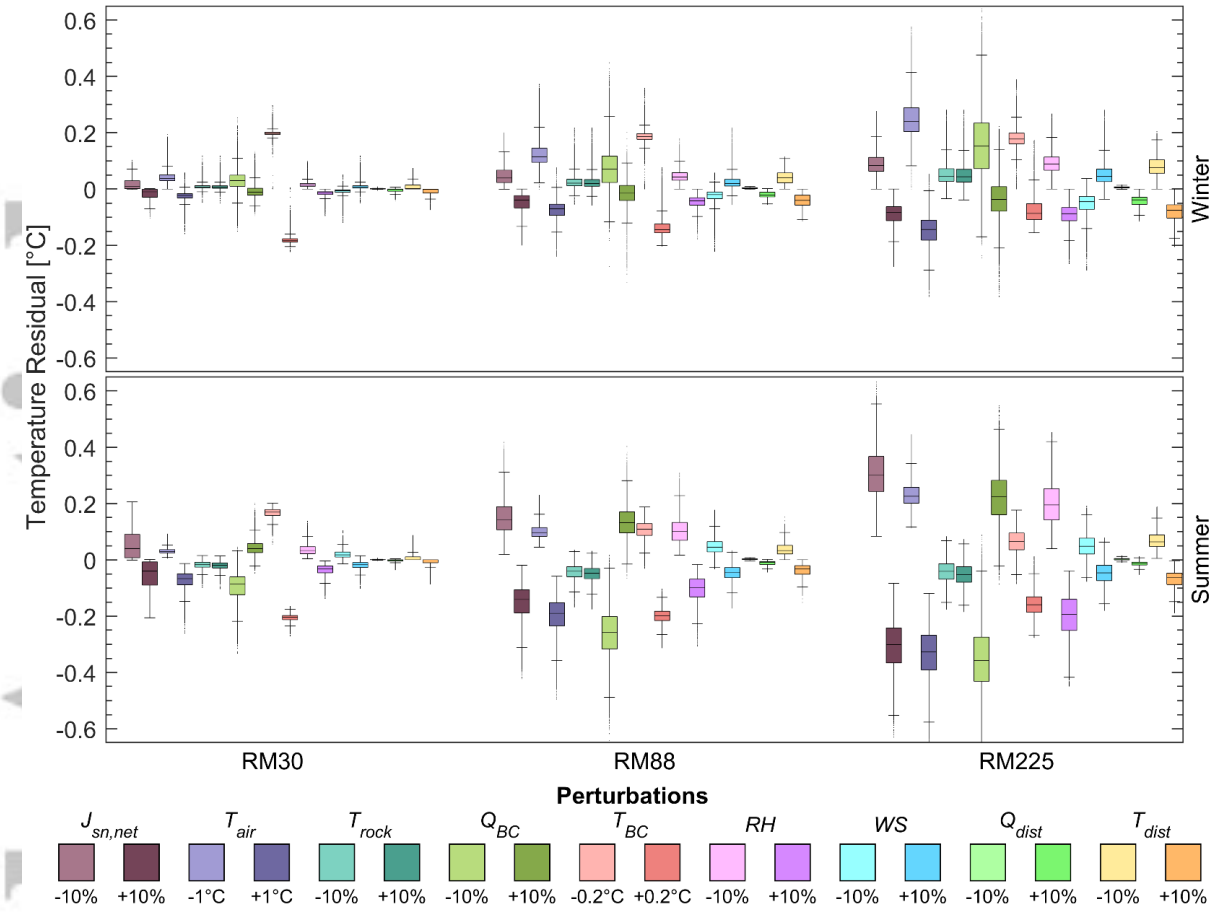

Figure 7. Sensitivity analysis of river temperature to input data perturbations at three locations during Winter and Summer averaged over the entire simulation time (Winter = Dec.-Feb., Summer = Jun.-Aug.). The residual is calculated as the detailed model minus scenario. Variables being compared are net shortwave radiation ($J_{sn,net}$), air temperature (T_{air}), rock temperature (T_{rock}), upstream boundary flow (Q_{BC}), upstream boundary condition temperature (T_{BC}), relative humidity (RH), wind speed (WS), distributed flows (Q_{dist}), distributed flow temperatures (T_{dist}). Box plot order follows that of the legend. Figure S10 depicts sensitivity analysis results for Spring and Fall.

Table 1. Statistics for modeled external heat fluxes (W/m^2) and percent of total external heat fluxes for the Colorado River in Grand Canyon between Jan 1, 2000 and Jan 1, 2018. Statistics for the relative contribution (%) were calculated from the absolute values for each heat flux over space and time divided by the sum of absolute values for all heat fluxes over space and time.

		$J_{sn,dir}$	$J_{sn,diff}$	$J_{sn,refl}$	J_{an}	J_{br}	J_{rock}	J_e	J_c	J_f	J_{sed}	J_{trib}	J_{dist}
Heat Flux [W/m^2]	Min	0	0	0	116	-408	0	-722	-380	0	-3	-509	-2
	Mean	127	32	1	267	-365	10	-84	69	78	7	0	25
	Max	1009	404	7	393	-331	125	526	1062	2047	25	1475	769
Relative Contribution [%]	Min	0	0	0	5	9	0	0	0	0	0	0	0
	Mean	8	2	0	27	37	1	8	6	7	1	0	3
	Max	56	32	1	45	61	12	46	56	77	4	66	47